ABRO1 arrests cardiomyocyte proliferation and myocardial repair by suppressing PSPH

Tao Wang,[1,2,6] Lu-Yu Zhou,[1,6] Xin-Min Li,[1,6] Fang Liu,[3,6] Lin Liang,[4] Xin-Zhe Chen,[1] Jie Ju,[1] Murugavel Ponnusamy,[1] Kai Wang,[1] Cui-Yun Liu,[1] Kao-Wen Yan,[5] and Kun Wang[1,2]

[1]Institute for Translational Medicine, The Affiliated Hospital of Qingdao University, College of Medicine, Qingdao University, Qingdao 266021, China; [2]Key Laboratory of Birth Regulation and Control Technology of National Health Commission of China, Shandong Provincial Maternal and Child Health Care Hospital Affiliated to Qingdao University, Jinan 250014, China; [3]Center of Diabetic Systems Medicine, Guangxi Key Laboratory of Excellence, and Department of Anatomy, Guilin Medical University, Guilin 541004, China; [4]State Key Laboratory of Cardiovascular Disease, Heart Failure Center, Fuwai Hospital, National Center for Cardiovascular Diseases, Chinese Academy of Medical Sciences, Peking Union Medical College, Beijing 100037, China; [5]State Key Laboratory of Membrane Biology, Institute of Zoology, Chinese Academy of Sciences, Beijing 100101, China

The role of Abraxas 2 (ABRO1 or KIAA0157), a component of the lysine63-linked deubiquitinating system, in the cardiomyocyte proliferation and myocardial regeneration is unknown. Here, we found that ABRO1 regulates cardiomyocyte proliferation and cardiac regeneration in the postnatal heart by targeting METTL3-mediated m^{6}A methylation of *Psph* mRNA. The deletion of ABRO1 increased cardiomyocyte proliferation in hearts and restored the heart function after myocardial injury. On the contrary, ABRO1 overexpression significantly inhibited the neonatal cardiomyocyte proliferation and cardiac regeneration in mouse hearts. The mechanism by which ABRO1 regulates cardiomyocyte proliferation mainly involved METTL3-mediated *Psph* mRNA methylation and CDK2 phosphorylation. In the early postnatal period, METTL3-dependent m^{6}A methylation promotes cardiomyocyte proliferation by hypermethylation of *Psph* mRNA and upregulating PSPH expression. PSPH dephosphorylates cyclin-dependent kinase 2 (CDK2), a positive regulator of cell cycle, at Thr14/Tyr15 and increases its activity. Upregulation of ABRO1 restricts METTL3 activity and halts the cardiomyocyte proliferation in the postnatal hearts. Thus, our study reveals that ABRO1 is an essential contributor in the cell cycle withdrawal and attenuation of proliferative response in the postnatal cardiomyocytes and could act as a potential target to accelerate cardiomyocyte proliferation and cardiac repair in the adult heart.

INTRODUCTION

The mammalian neonatal cardiomyocytes have proliferating potential, which hastily declines after the postnatal period. In the adult heart, the withdrawal of cardiomyocytes cell cycle activity and its inability to proliferate, due to the loss of expression and/or activities of the cell cycle components, in particular the positive regulators of cell cycle,[1,2] is primarily responsible for the maladaptive repair, cardiac dysfunction, and heart failure following various insults.[3–5] Growing evidence demonstrates that a considerable number of cardiomyocytes in the adult heart retain the proliferative and regenerative capacity; however, the turnover number is not sufficient for the efficient cardiac repair and heart function after the loss of cardiomyocytes due to injury.[6] Several studies reveal that the induction or enforced expression of cell cycle proteins such as cyclins and cyclin-dependent kinase (CDK)[7–9] or attenuation of cell cycle inhibitors[10] can improve the cardiomyocyte cell cycle activity, productive cell division, and regenerative response to some extent in the adult heart. Despite substantial progress having been made to understand the cardiomyocyte cell cycle exit soon after birth, the cellular and molecular mechanisms underlying the activation and inactivation of cardiomyocyte proliferation are still largely unknown in the mammalian heart.

Abraxas brother 1 (ABRO1) is a part of the BRCC36-containing isopeptidase (BRISC) complex and functions as a scaffold protein in the BRISC complex, which recruits proteins required for complex assembly and regulating its catalytic activity.[11,12] ABRO1 has been reported to participate in important biological and pathological processes. For example, ABRO1 regulates DNA damage response, suppresses tumorigenesis,[13] and promotes NLRP3 inflammasome activation through mediation of NLRP3 deubiquitination.[14] ABRO1 is indicated to maintain genome stability and limits replication stress.[15] ABRO1 negatively regulates cell cycle progression,[13] and our previous experiment also indicated that ABRO1 is required for proper mitosis and cell division.[16] Moreover, ABRO1 predominantly expresses in the

(legend on next page)

heart and its level is regulated upon myocardial ischemia/reperfusion (I/R) injury,[17] indicating that ABRO1 plays a critical role in hearts. To date, the function of ABRO1 in the heart remains largely unexplored, so we wanted to unveil whether ABRO1 participates in the regulation of cardiomyocyte proliferation.

The cardiomyocyte proliferative response has a distinct gene transcription and post-transcriptional program.[18–20] Recent studies reveal that N6-methyladenosine (m^{6}A) modification of RNA transcripts, a prevalent form of post-transcriptional modification of mRNA, has a significant impact on cardiac gene expression, cell proliferation, and growth by modulating RNA stability and translation.[21–24] Post-translational modifications of proteins are associated with cell cycle activity and proliferation, which have indispensable roles in regulating both cardiomyocyte cell proliferation and growth as well as cardiac diseases.[25–28] The gene expression program that regulates cardiac proliferation is an integrated network composed of transcriptional, post-transcriptional, and post-translational components, and the identification of molecules that function as master regulators of many signaling pathways would be beneficial to re-establish cardiomyocytes and boost cardiac regeneration in the injured adult heart.

Here, we show that ABRO1 is a critical regulator of cardiomyocyte proliferation in postnatal hearts. Using genetic deletion and overexpression approach, we demonstrate that ABRO1 suppresses cardiomyocyte cell cycle activity by directly interacting with methyltransferase-like 3 (METTL3) and inhibiting its RNA N6-adenosine methylation (m^{6}A) activity, which leads to the downregulation of phosphoserine phosphatase (PSPH) expression through hypomethylation of PSPH mRNA and attenuation of PSPH-dependent activation of CDK2, the positive regulator of the cell cycle. Thus, our study reveals that METTL3-dependent RNA m^{6}A modification has a significant contribution in the cardiomyocyte proliferation and cardiac regenerative response by upregulating cell cycle protein activity, but ABRO1 deteriorates its function and revokes the proliferating ability of cardiomyocytes in the postnatal as well as in adult heart.

RESULTS

ABRO1 negatively regulates cardiomyocyte proliferation in postnatal and adult hearts

To understand the role of ABRO1 in cardiomyocyte proliferation and myocardial regeneration, we first examined the expression pattern of ABRO1 protein in the postnatal hearts of mice under physiological conditions and found that the level of ABRO1 protein in the myocardial tissue was relatively low at birth, significantly increased from P1 to P7 (Figure S1A), and highly expressed during the adulthood (at P30 and P90) (Figure 1A). In the adult mice, ABRO1 protein was abundantly expressed in the kidney and heart (Figure 1B) and was significantly higher in cardiomyocytes than in fibroblasts (Figure S1B). To investigate the function of ABRO1 in cardiomyocyte proliferation and myocardial regeneration, we generated Abro1 knockout (ABRO1 KO) mice using the CRISPR-Cas9 gene-editing system (Figures 1C and S1C-S1E; Table S1). The deletion of Abro1 was confirmed by PCR assay (Figure 1D) and western blot analysis (Figure 1E) in mouse hearts. The knockout of Abro1 did not affect the heart function, heart to body weight ratio, and morphology of cardiac tissue compared with their littermate control mice at P12 (Figures S2A–S2C). However, the cardiomyocyte proliferation as indicated by 5-ethynyl-2′-deoxyuridine (EdU; labels cells passing through S phase)-positive, histone H3 phosphoserine 10 (pH3, a mitosis marker)-positive, and aurora B kinase (Aurora B, a cytokinesis marker)-positive cardiomyocytes were higher in Abro1-deleted postnatal hearts (Figures S2D–S2F). In adult hearts, the knockout of Abro1 had similar effects on heart function (Figures 1F, S3A–S3C), morphology of cardiac tissue (Figures 1G and 1H), and cardiomyocyte proliferation (Figures 1I–1K and S3D) under physiological conditions. Further, cardiomyocyte cell sizes at P12 and P60 were reduced (Figures S3E and S3F), and no hypertrophic effects were observed in adult ABRO1 KO mouse hearts (Figures S3G and S3H).

Next, we isolated cardiomyocytes from adult mouse heart and performed nucleation and ploidy analysis. The percentages of mononuclear cardiomyocytes and diploid cardiomyocytes were increased in ABRO1 KO mouse hearts, while the percentage of polyploid cardiomyocytes was reduced (Figures S4A–S4C). In addition, the ABRO1 KO mice had a significant elevation in diploid cardiomyocyte subpopulation in mononuclear cardiomyocytes (Figure S4D). The results indicate that ABRO1 deficiency increases karyokinesis, and thereby reduces ploidy. We further examined the role of ABRO1 on kidney and found that there were no significant detectable effects on kidney morphology and function in ABRO1 KO mice compared with wild-type (WT) mice (Figures S5A–S5C). Together, these results indicate that the upregulation of ABRO1 expression in postnatal and adult hearts is associated with the obstruction of cardiomyocyte proliferation.

Figure 1. ABRO1 regulates cardiomyocyte proliferation in postnatal and adult hearts

(A) Representative western blots (top) and statistical data (bottom) showing the expression of ABRO1 in hearts at different ages of mice: P1, P7, P30, and P90 (n = 5 mice). (B) The expression level of ABRO1 protein and statistical data in different tissues of adult mice (n = 4 mice). (C) A schematic diagram illustrating the deletion of Abro1 using the CRISPR-Cas9 genome editing method. The deleted region in Abro1 gene and spanning region of primers (forward [F1] and reverse [R1, R2]) used for the detection of ABRO1 knockout (ABRO1 KO) are shown. (D and E) PCR assay showing the deletion of Abro1 in mouse hearts (D) and western blot image (top) and statistical data (bottom) showing the myocardial level of ABRO1 (E) in wild type (WT) and ABRO1 KO at P60 (n = 9 mice). (F–K) ABRO1 KO increases cardiomyocyte proliferation in adult mouse hearts (at P60). Echocardiography analysis of fractional shortening (FS) (F) and heart weight to tibia length (HW/TL) ratio (G) in WT and ABRO1 KO mice (n = 6–8 mice). (H) Representative images of gross morphology and hematoxylin-eosin-stained transverse sections of hearts from WT and KO mice (scale bar, 2 mm). (I) Immunostaining for cardiac troponin T (cTNT, green) and nucleus (DAPI, blue) in EdU (red, white arrow) infused heart sections (scale bar, 25 μm), and the quantification of EdU-positive cardiomyocytes (right) was calculated (n = 6 mice per group). (J) Representative confocal images and quantification of pH3-positive cardiomyocytes (red, white arrow; scale bar, 25 μm) in WT and ABRO1 KO hearts. cTNT-marked cardiomyocytes and DAPI-labelled nuclei (n = 7 mice per group). (K) Aurora-B-positive cardiomyocytes were calculated in WT and ABRO1 KO hearts (n = 6 mice per group). All data are mean ± SD.
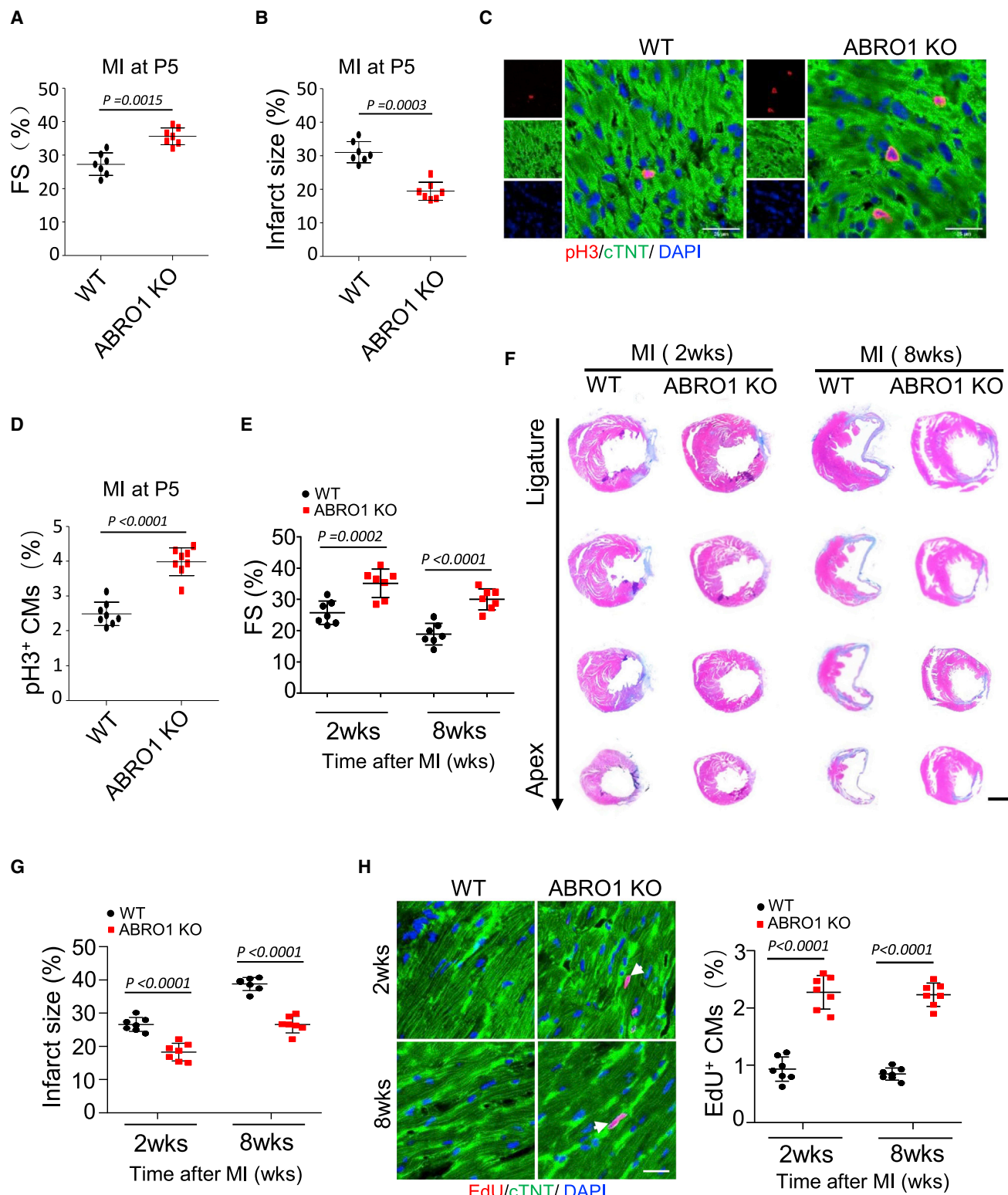
Figure 2. ABRO1 deletion promotes cardiomyocyte proliferation and improves cardiac function following MI injury

(A–D) The neonatal ABRO1 KO mice (P5) and WT mice (P5) were subjected to MI. (A) Echocardiography analysis of FS at 3 days after MI (n = 7 mice per group). (B) Analysis of the percentage of the infarct size (n = 7 mice per group). (C and D) Representative confocal images and quantification of pH3-positive cardiomyocytes in heart sections at

(legend continued on next page)

ABRO1 deletion accelerates cardiomyocyte proliferation and cardiac regeneration after myocardial infarction

Unlike the neonatal heart, the adult heart loses its regenerative capacity mainly due to the lack of cardiomyocytes with proliferating ability.[29–31] To further investigate the impact of ABRO1 deletion on the cardiomyocyte proliferation and cardiac regeneration in postnatal and adult hearts, ABRO1 KO and WT mice were subjected to myocardial infarction (MI) (by left anterior descending artery ligation) at P5 and at P60. The knockout of *Abro1* ameliorated left ventricle function (Figure 2A), reduced MI-induced infarct size (Figure 2B), and also promoted cardiomyocyte proliferation (Figures 2C and 2D) compared with WT mice at P5. In adult hearts, echocardiography analysis at 2 and 8 weeks after MI showed that the left ventricle function was significantly improved in ABRO1 KO mice compared with WT mice (Figure 2E). The loss of ABRO1 also reduced MI-induced increased of infarct size (Figures 2F and 2G), and the number of EdU-positive cardiomyocytes was higher in ABRO1 KO hearts at 2 weeks and 8 weeks after MI injury (Figure 2H). This result suggests that the depletion of ABRO1 attenuates MI through cardiomyocyte proliferation. Furthermore, terminal deoxynucleotidyl transferase dUTP nick end labeling (TUNEL) assays showed that ABRO1 had no effects on apoptosis in cardiomyocytes (Figures S6A and S6B) and in the heart (Figure S6C) under basal conditions. ABRO1 expression was elevated in adult mice after MI (Figure S6D), and there was no detectable difference in the level of apoptosis in ABRO1 KO and WT hearts (Figures S6E and S6F), indicating that the acceleration of cardiomyocyte proliferation may be the underlying mechanism of the reduced infarct size in ABRO1 KO mouse hearts. Collectively, these results suggest that ABRO1 contributes to the blockage of cardiomyocyte proliferation during the postnatal developing heart, and suppression of ABRO1 improves myocardial repair and cardiac function after MI injury mainly through the induction of cardiomyocyte proliferation.

Overexpression of ABRO1 inhibits cardiomyocyte proliferation and cardiac regeneration in neonatal and adult hearts

Next, we sought to confirm whether the upregulation of ABRO1 is involved in the obstruction of cardiomyocyte proliferation. Under physiological condition, the overexpression of ABRO1 (ABRO1 OE) in postnatal hearts at P7 (Figures S7A and S7B) did not affect the left ventricular function, heart mass, and cardiac morphology (Figures S7C–S7E). There was no significant difference of cardiac function (Figure 3A), heart mass (Figure 3B), and morphology (Figure 3C) in ABRO1-overexpressed adult hearts (Figures S8A and S8B). However, the cardiomyocyte size (Figure 3D) was larger and cardiomyocyte proliferation (Figures S8C and S8D) was decreased in the adult hearts of mice overexpressing ABRO1 compared with WT hearts. Besides, the enforced expression of ABRO1 reduced pH3-positive cardiomyocytes (Figure 3E) at P7. To further confirm the

ABRO1-mediated inhibition of cardiomyocyte proliferation, neonatal mice (postnatal day 1 [P1]) were administered with ABRO1 and subjected to MI. In mice overexpressing ABRO1, the cardiomyocytes with pH3 were reduced (Figure 3F), the infarct size was remarkably higher (Figures 3G and 3H), and left ventricular function was reduced (Figure 3I) at P7 following MI injury. Together, these results indicate that postnatal expression of ABRO1 is associated with cardiomyocyte cell cycle exit, and upregulation of ABRO1 hinders cardiac regeneration by promoting proliferation arrest of cardiomyocytes in postnatal hearts.

ABRO1 regulates cardiomyocyte proliferation *in vitro*

To further confirm that ABRO1 regulates cardiomyocyte proliferation, neonatal cardiomyocytes were infected with adenoviral vector harboring Abro1 specific short hairpin RNA (shRNA) (ABRO1-shRNA) or mouse Abro1 gene (ABRO1 OE). The knockdown of ABRO1 significantly reduced the levels of Abro1 mRNA and protein in neonatal cardiomyocytes (Figures 4A and 4B). The suppression of ABRO1 enhanced proliferating cardiomyocyte number as indicated by increased EdU-positive cells (Figure 4C). In addition, the cardiomyocytes with a mitotic marker (pH3) and cytokinesis marker (Aurora B) were markedly increased in ABRO1-silenced cardiomyocytes (Figures 4D and 4E). In contrast, enforced expression of ABRO1 in neonatal cardiomyocytes (Figures 4F and 4G) reduced proliferating cardiomyocytes, which is evident from a significant reduction of pH3-positive (Figure 4H) and Aurora B-positive (Figure 4I) cardiomyocytes. These data confirmed that the upregulation of ABRO1 restrains cell cycle progression and proliferation of cardiomyocytes, while ablation of ABRO1 can promote cardiomyocyte proliferation.

ABRO1 interacts with METTL3 and affects its RNA m^{6}A methylation function

To elucidate the molecular mechanism of ABRO1-dependent regulation of cardiomyocyte proliferation, we first investigated the proteins interacting with ABRO1. It has been reported that ABRO1 was associated with p53 and spindle assembly, and thus we checked the effects of ABRO1 on p53 expression. The results indicated that ABRO1 is not involved in the regulation of p53 expression (Figures S9A and S9B). YAP is a core regulator of cardiac regeneration, so we tested whether ABRO1 could regulate the expression of YAP. The results showed that ABRO1 did not participate in the regulation of YAP (Figures S9C and S9D). Next, we carried out protein immunoprecipitation (IP) assay in isolated cardiomyocytes using FLAG-tagged ABRO1 and FLAG-control. The ABRO1-IP materials and its control were resolved using SDS-PAGE gel, and the entire gel lanes of ABRO1-IP materials and its control were excised and sent for liquid chromatography-tandem mass spectrometry (LC-MS/MS) analysis. Among the proteins enriched in FLAG-tagged ABRO1, we identified

3 days after MI (n = 8 mice per group). (E–H) Ten-week-old ABRO1 KO and WT mice were subjected to MI (MI at 10 weeks) and heart samples were collected at 2 weeks and 8 weeks post MI. (E) Echocardiography analysis of left ventricular function (FS%) after MI (n = 7 mice). (F) Representative images of Masson's trichrome-stained cross sections of hearts (scale bar, 2 mm). (G) Quantification of the left ventricle infarct size measured as the percentage of epicardial and endocardial infarct arc length at 2 weeks and 8 weeks post MI (n = 7 mice per group). (H) Immunostaining for cTNT (green) and nucleus (DAPI, blue) in EdU (red, white arrow) infused heart sections (scale bar, 25 μm), and the EdU-positive cardiomyocytes were calculated (n = 7 mice per group). All data are mean ± SD.
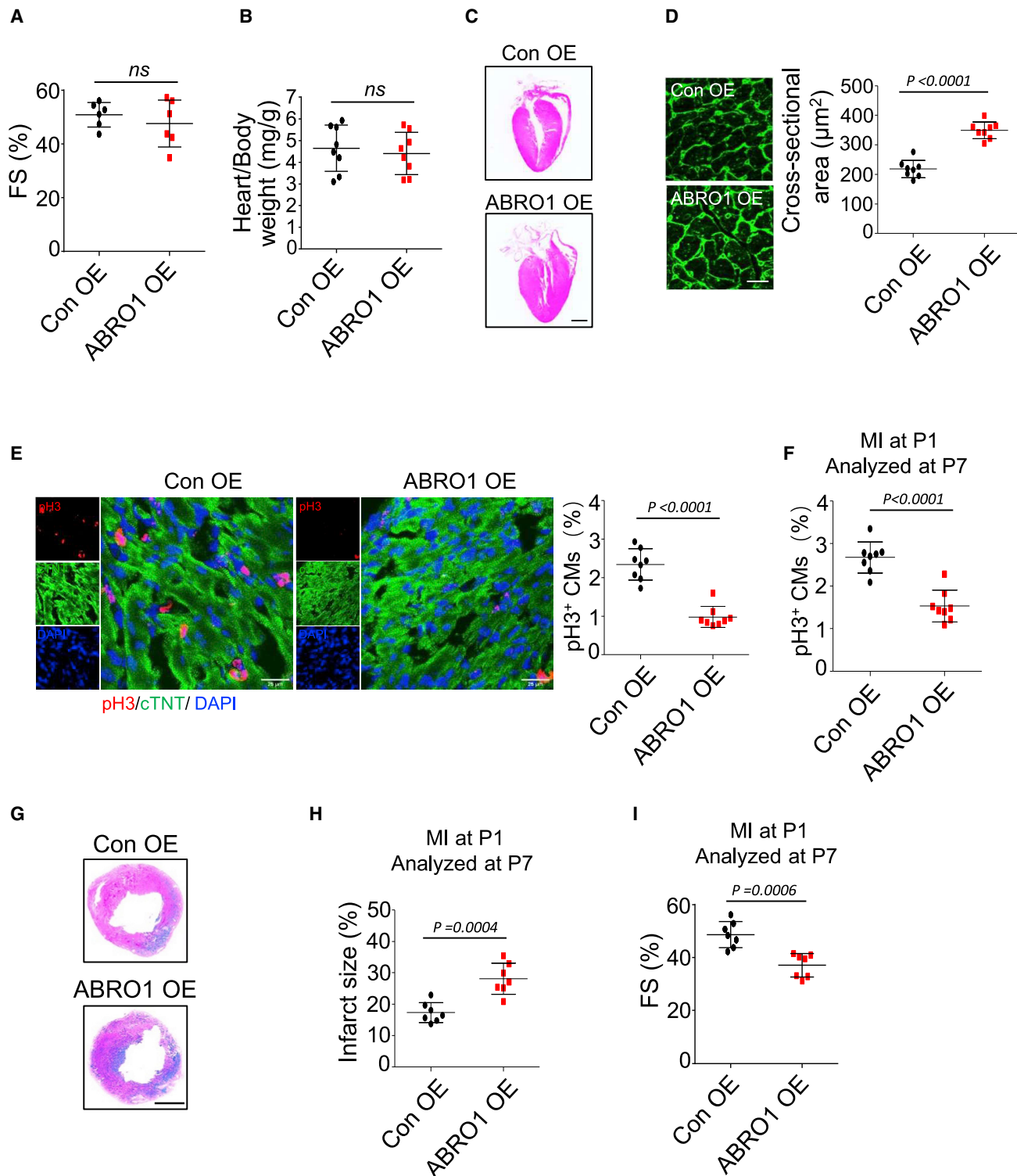
Figure 3. ABRO1 OE inhibits cardiomyocyte proliferation and cardiac regeneration in neonatal hearts

(A–D) AAV9 vector carrying Abro1 (ABRO1 OE) or negative control (Con OE) were administered to adult WT mice. The left ventricular FS% (A) and heart to body weight ratio (B) were measured at 21 days after AAV9 administration (n = 6–8 mice per group). (C) Representative images of hematoxylin-eosin-stained transverse sections of hearts at 21 days post AAV9 administration (scale bar, 2 mm). (D) Wheat germ agglutinin (WGA) staining of ventricular sections (scale bar, 20 μm) (left) and cardiomyocyte

(legend continued on next page)

that METTL3, the RNA methyltransferase that specifically methylates N6-adenosine, was enriched in FLAG-ABRO1 (Figure 5A). The study confirmed that METTL3-mediated N6-adenosine mRNA methylation is a dynamic modification that is necessary for the response to cardiac hypertrophy. However, the effect of METTL3 in cardiomyocyte proliferation remains unclear, and thus we focused on METTL3 for further studies. The interaction between ABRO1 and METTL3 was verified by immunoprecipitation with METTL3 and ABRO1 antibodies followed by western blot (Figures 5B, 5C, S10A, and S10B). Interestingly, the mRNA and protein levels of METTL3 were not altered by overexpression of ABRO1 in cardiomyocytes (Figures S10C and S10D) and knockout of ABRO1 did not affect the expression levels of METTL3 mRNA or protein compared with that of WT hearts (Figures S10E and S10F), indicating that ABRO1 could possibly affect METTL3 m^6A activity. Together, these data suggest that ABRO1 interacts with METTL3, and this interaction might regulate the m^6A methylation activity of METTL3 in cardiomyocytes.

Transcriptome-wide m^6A methylation analysis to identify targets of ABRO1

We next sought to assess the m^6A modifications in mRNA, and the m^6A-seq analysis was carried out in WT and ABRO1 KO hearts (Table S2). The analysis of the distribution of m^6A peak density in mRNA transcripts showed that m^6A peaks are mainly found in coding sequences (CDSs), and a considerable amount of m^6A peaks enriched around start codon and stop codon regions in mRNA transcripts from ABRO1 KO and WT hearts. However, the density of the peaks was not significantly altered in all three main segments (5′ UTR, CDS, 3′ UTR) of mRNA transcripts from ABRO1 KO mice heart compared with WT heart (Figures 5D and S11A). Among the total RNA transcripts with m^6A sites, more than half (59.4%) of mRNA transcripts contained ≤2 m^6A peaks, 27.4% of mRNA transcripts comprised 3 to 5 m^6A peaks, and more than five m^6A peaks existed in 13.2% of mRNA transcripts (Figure S11B). The sequence motif analysis of m^6A-containing peaks showed that those peaks are highly enriched with a conserved consensus motif sequence of METTL3 (GGACU) (Figure 5E). Further, MeRIP sequencing (MeRIP-seq) analysis results from adult ABRO1 KO hearts showed that a total of 3,444 m^6A peaks were upregulated and 4629 m^6A were downregulated compared with WT hearts (Figure 5F; Table S2). Next, we performed RNA sequencing (RNA-seq) analysis and observed that a total of 364 mRNAs were upregulated and 668 mRNAs were downregulated in ABRO1 KO hearts compared with WT hearts (Figure S11C; Table S3). To sort out the gene expression level according to the m^6A modifications, we plotted differentially expressed genes

(from RNA-seq data) against m^6A peaks data (from MeRIP-seq) (Table S4). We termed increased m^6A modification (FC ≥ 1.5) as hypermethylated and decreased m^6A modification (FC ≤ 1.5) as hypomethylated, respectively, and found that 17 hypermethylated mRNAs were upregulated, eight hypermethylated mRNAs were downregulated, three hypomethylated mRNAs were upregulated, and 91 hypomethylated mRNAs were downregulated in ABRO1 KO hearts compared with WT hearts. (Figure 5G). Collectively, these results reveal that ABRO1 might regulate METTL3-mediated m^6A methylation of mRNA transcripts of genes that are involved in the inhibition of cardiomyocyte proliferation.

ABRO1 KO promotes METTL3-dependent m^6A methylation of PSPH mRNA and its expression

We anticipated that ABRO1 interaction blocks m^6A methyltransferase activity of METTL3, and differentially expressed m^6A-hypermethylated mRNAs in ABRO1-silenced hearts could be the potential downstream target(s) of METTL3 during cardiomyocyte proliferation. Based on the deregulated genes, we observed that PSPH had the highest m^6A modification and the mRNA level of PSPH was highly increased in ABRO1 KO hearts among the potential target genes of METTL3-mediated m^6A methylation. The Integrative Genomics Viewer (IGV) analysis of PSPH mRNA showed that there was a remarkable increase of m^6A peaks along with a significant increase of PSPH mRNA level in ABRO1 KO heart (Figure 6A). m^6A RNA immunoprecipitation (RIP) qPCR results further confirmed the increase of m^6A modification (Figure 6B) along with an increase of PSPH mRNA (Figure 6C) and protein (Figure 6D) in ABRO1 KO hearts compared with WT hearts. In contrast, the m^6A modification in PSPH mRNA was decreased (Figure S12A) along with a decrease in the levels of PSPH mRNA and protein in ABRO1-treated cardiomyocytes (Figures S12B and S12C). In addition, the binding of PSPH mRNA to METTL3 was significantly enriched in ABRO1 KO mouse hearts (Figure 6E). Interestingly, PSPH can positively regulate cell cycle progression and cell proliferation.[32,33] This prompted us to select PSPH for further assessment as a potential downstream target of ABRO1-METTL3 in the cardiomyocyte proliferation. Next, we examined the function of ABRO1-mediated suppression of PSPH expression in neonatal cardiomyocytes, which have proliferating ability. The expression of PSPH was significantly decreased by PSPH-shRNA transfection in cardiomyocytes (Figure 6F). The silencing of ABRO1 using ABRO1-shRNA increased cardiomyocytes with the mitotic marker (pH3), and this effect was abolished upon PSPH-shRNA along with ABRO1-shRNA in cardiomyocytes (Figure 6G). We examined PSPH expression in the heart and found that the level of PSPH protein in the myocardial tissue was significantly decreased

surface area (right) was measured at 21 days post AAV9 administration (n = 8 mice per group). (E) Adenovirus harboring *Abro1* (ABRO1 OE) or negative control (Con OE) were administered to WT mice (at P1) and samples were collected at day 7 (P7). Representative confocal images of heart sections co-stained with pH3 (red), cTNT (green), and the nucleus (DAPI, blue) (scale bar, 25 μm) (left), and pH3-positive (right) cardiomyocytes were calculated (n = 8 mice per group). (F–I) The neonatal mice (P1) were administered with adenoviral ABRO1 (ABRO1 OE) or negative control (Con OE) and subjected to MI. (F) Quantification of the number of pH3-positive cardiomyocytes in heart sections at 7 days after MI (n = **8** mice per group). (G) Representative images of Masson's trichrome-stained cross sections of hearts (scale bar, 2 mm). (H) The infarct size was quantified using length-based measurements at P7 post MI (n = 7 mice per group). (I) Echocardiography analysis of FS (n = 7 mice per group) at P7 post MI. All data are mean ± SD.

A

B

C

EdU/cTNT/ DAPI

D

pH3/cTNT/ DAPI

E

Aurora B/cTNT/ DAPI

F

G

H

I
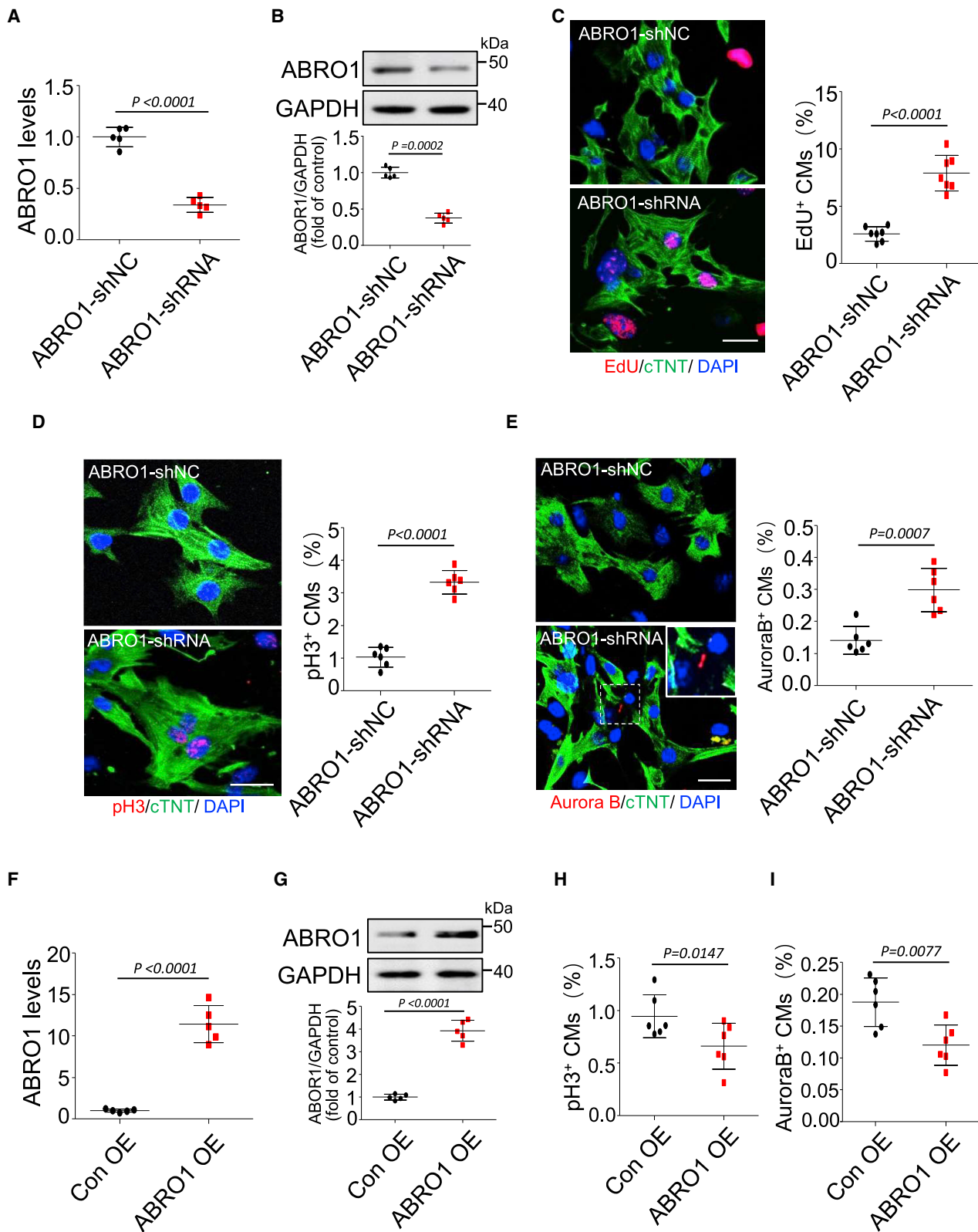
(legend on next page)

from birth to adulthood (Figure S12D). The enforced expression of PSPH (using the AAV9 system) in adult mouse hearts improved cardiac function, reduced infarct size, and produced higher proliferating cardiomyocytes in MI-injured hearts compared with WT hearts with MI injury (Figures 6H-6J), which indicates that PSPH is involved in cardiomyocyte proliferation and cardiac regeneration.

We further investigate the function of METTL3 in the regulation of cardiomyocyte proliferation, and validated the mechanistic link between ABRO1 and METTL3. In cardiomyocytes, METTL3 silencing reduced cardiomyocyte proliferation (Figures S13A and S13B). Conversely, the enforced expression of METTL3 induced an increase in cardiomyocyte proliferation, and this increase was reversed upon ABRO1 OE (Figures S13C and S13D). Further, METTL3 inhibition blocked ABRO1 knockdown-induced increase of cardiomyocyte proliferation (Figures S13E and S13F), while METTL3 overexpression attenuated the effects of ABRO1 in cardiomyocyte proliferation (Figures S13G and S13H). *In vivo*, ABRO1 deletion-induced proliferative effects were reversed upon silencing METTL3 (Figures S14A and S14B). These results reveal the role of METTL3 in the regulation of cardiomyocyte proliferation and validated the relationship between ABRO1 and METTL3 on cardiomyocyte proliferation. In addition, USP5 has recently been shown to stabilize METTL3 expression, thus contributing to the decrease of pluripotent factor transcripts and the proper embryonic stem cell (ESC) differentiation programming of stem cells.[34] We then explored whether USP5 is involved in the pathway of ABRO1-mediated cardiomyocyte proliferation. Our results showed that knockdown of USP5 did not affect the expression levels of METTL3 in cardiomyocytes (Figure S14C), and the interaction between USP5 and METTL3 was not observed by immunoprecipitation with USP5 and METTL3 antibodies followed by western blot in cardiomyocytes (Figures S14D and S14E). Together, these results rule out the involvement of USP5 in this proposed mechanism.

ABRO1-mediated expression of PSPH promotes dephosphorylation of CDK2 and proliferation of cardiomyocytes

PSPH primarily functions as a dephosphorylating enzyme, which can regulate several signaling pathways by modulating the phosphorylation status of protein molecules.[32,33,35,36] To explore the phosphoproteins regulated by PSPH that involved in positive modulation of cardiomyocyte proliferation, we performed phosphoproteome analysis. In PSPH-silenced cardiomyocytes, a total of 3,322 proteins were quantified from all identified proteins (3,684) and detected peptides (12,621). From 8,923 phospho-modified peptides, 8,828 phospho-sites were quantified among all identified phospho-sites (10,531 sites) (Figure S15A). Among the quantified proteins, 309 phosphoproteins were differentially expressed (184 upregulated and 125 downregulated) (Figures 7A and S15B; Table S5) in PSPH-silenced cardiomyocytes. While 376 phosphorylation sites were significantly modified (200 sites upregulated and 176 sites downregulated) among the quantified sites (8,828), corresponding to 8,923 phospho-modified peptides in PSPH knockdown cardiomyocytes compared with control (Figure S15B). The length distribution of most of the identified phosphopeptides was between >8 and <20 residues (average length ~14), which is the standard property of tryptic peptides (Figure S15C). In PSPH-silenced cardiomyocytes, the number of phosphorylation sites was varied in proteins and most of the proteins contain fewer than five phosphorylation sites. Half (~52%) of the all quantified phosphoproteins contained only one phosphosite, while ~23% and ~12% of proteins consisted of two and three phosphorylation sites, respectively. Nearly 13% of phosphoproteins had more than three phospho-sites (Figure S15D).

Among these significantly phospho-modified and upregulated phosphorylated proteins, we found that CDK2 have T14 and Y15, two phospho-modified sites, and was the top-hit cell cycle-related protein based on the Gene Ontology (GO) analysis. Hence, our further studies were focused on the influence of ABRO1 and PSPH on CDK2 phosphorylation. CDK2 has two highly conserved neighboring phosphorylation sites (Thr14 and Tyr15), which have inhibitory action on CDK2 activity.[37,38] The knockdown of PSPH remarkably increased phosphorylation of Thr14/Tyr15 in CDK2, and PSPH overexpression dramatically decreased Thr14/Tyr15 phosphorylation in CDK2 without altering total CDK2 level in cardiomyocytes (Figures 7B, 7C, S16A, S16B, and S17A–S17H). Similarly, the ABRO1 deficiency significantly decreased phosphorylation of CDK2 at Thr14/Tyr15 in myocardial tissues of mice, while ABRO1 OE significantly increased Thr14/Tyr15 phosphorylation in CDK2 in cardiomyocytes (Figures 7D, 7E, and S18A–S18F). To confirm that ABRO1-mediated suppression of PSPH is involved in dephosphorylation of Thr14 and Tyr15 in CDK2, we transfected cardiomyocytes with ABRO1-shRNA in the presence or absence of PSPH-shRNA. As expected, ABRO1-shRNA-induced reduction of phosphorylation of Thr14/Tyr15 was

---

Figure 4. ABRO1 controls cardiomyocyte proliferation *in vitro*

(A–E) Neonatal mouse cardiomyocytes were infected with adenovirus harboring ABRO1-shRNA or scrambled control (ABRO1-shNC) for 48 h. (A) The expression levels of *Abro1* mRNA assessed by qRT-PCR (n = 5 independent experiments). (B) Representative western blots (top) and statistical data (bottom) showing the expression of ABRO1 (n = 5 independent experiments). (C) Representative confocal images of EdU-positive cardiomyocytes (scale bar, 20 μm) and quantification of EdU-positive (right) cells (n = 7 independent experiments). (D) Representative confocal images of pH3-positive cardiomyocytes and quantification of pH3-positive cells in ABRO1-shNC and ABRO1-shRNA infected cardiomyocytes (scale bar, 20 μm) (n = 6 independent experiments). (E) Representative confocal images of aurora B-marked cardiomyocytes and quantification of aurora-B-positive cells in ABRO1-shNC and ABRO1-shRNA infected cardiomyocytes (scale bar, 20 μm) (n = 6 independent experiments). (F–I) Neonatal mouse cardiomyocytes were infected with adenovirus harboring negative control (Con OE) or mouse *Abro1* gene (ABRO1 OE) for 48 h. (F) The expression levels of *Abro1* mRNA determined by qRT-PCR (n = 5 independent experiments). (G) Representative western blots (top) and statistical data (bottom) showing the expression of ABRO1 (n = 5 independent experiments). (H) pH3-positive cardiomyocytes were measured in Con OE- and ABRO1 OE-treated cardiomyocytes (n = 6 independent experiments). (I) Aurora B-marked cardiomyocytes were measured in Con OE- and ABRO1 OE-treated cardiomyocytes (n = 6 independent experiments). All data are mean ± SD.
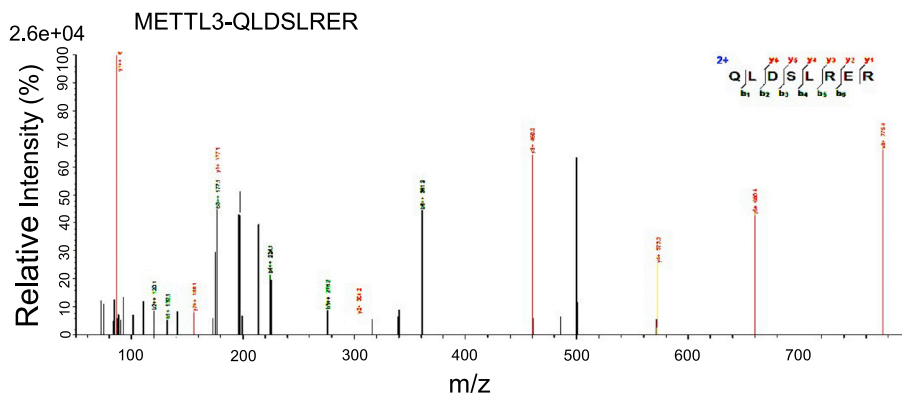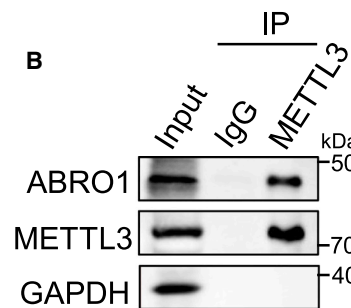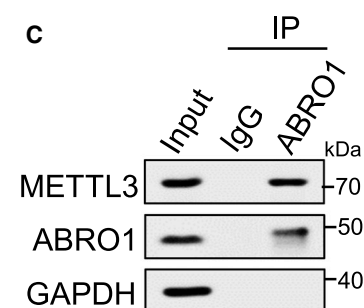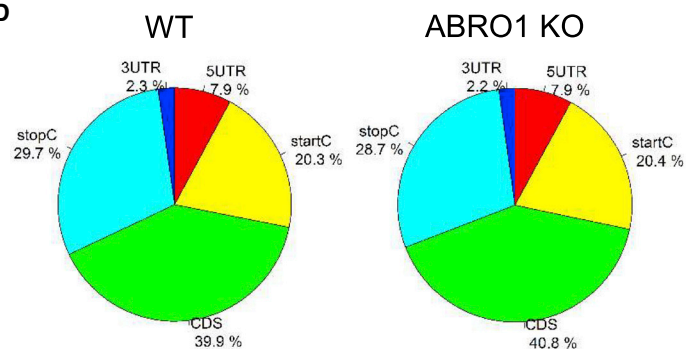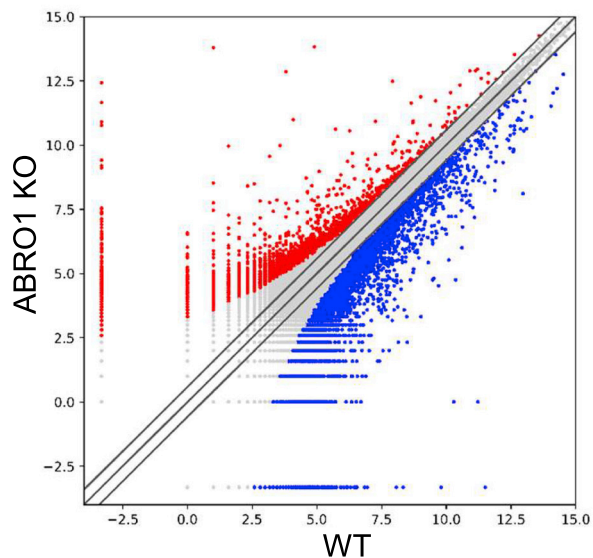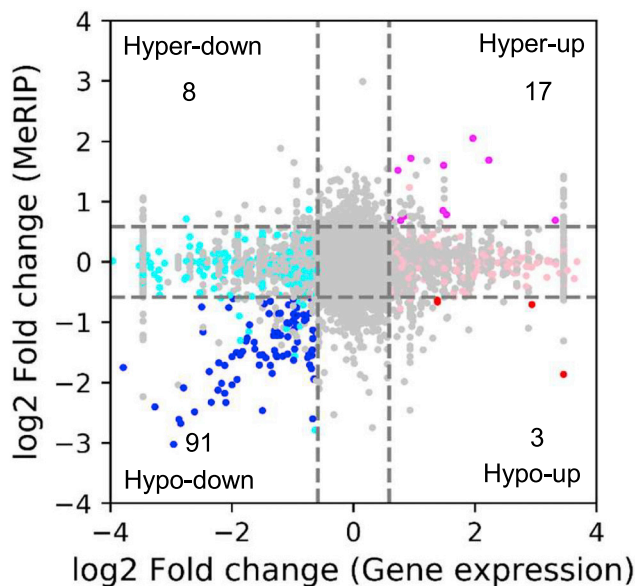
(legend on next page)

attenuated upon PSPH-shRNA exposure (Figures 7F and S18G–S18I). Together, these results suggest that ABRO1-mediated suppression of PSPH, through m⁶A hypomethylation, attenuates CDK2 activity by upregulating Thr14 and Tyr15 phosphorylation, which results in impediment to postnatal cardiomyocyte proliferation and regeneration.

DISCUSSION

In mammalians, the molecular mechanisms associated with cell cycle withdrawal and inherent non-proliferative growth of cardiomyocytes during postnatal life is a largely unknown phenomenon. In this study, we demonstrate that ABRO1 participates in the postnatal cardiomyocyte proliferation arrest and impairment of cardiac regeneration following injury in the adult heart. In the postnatal heart, ABRO1 interacts with METTL3 and inhibits its activity. METTL3-induced PSPH mRNA m⁶A methylation makes PSPH mRNA more stable and increases PSPH mRNA and protein expression level. Then, PSPH induces dephosphorylation of inhibitory phospho-sites (Thr14/Tyr15) in CDK2, a crucial cell cycle protein, which finally leads to cell proliferation (Figure 7G). Our study exemplifies that METTL3-dependent m⁶A RNA hypermethylation of genes is involved in cardiomyocyte proliferation; however, the substantial expression of ABRO1 beyond the postnatal period intervenes in this event and halts the cardiomyocyte proliferative response.

In mammals, including human and mouse, ABRO1 is abundantly expressed in cardiomyocytes, and it protects the cardiomyocytes from death.[17] However, its functional impact on cardiomyocyte proliferation remains elusive. We found that the ABRO1 level in the myocardial tissue is remarkably low during the early postnatal period and higher in young and adult hearts, and this upregulation negatively regulates cardiomyocyte proliferation. It is well documented that ABRO1 negatively regulates cell cycle progression.[13,16] However, the BRISC complex, in which ABRO1 is an integral component, is required for proper mitosis and cell division.[16] Our study found that the enforced expression of ABRO1 impedes proliferative response and cardiac repair in neonatal cardiomyocytes and hearts. Most importantly, the silencing or deletion of Abro1 amplified regenerative responses, improved cardiac function, and reduced infarct size, which is mainly achieved through the acceleration of cardiomyocyte proliferation. ABRO1, together with the BRISC complex, is conventionally involved in lys63-specific deubiquitylation, which is a non-proteolytic event modulating the biological activity of proteins. ABRO1 can directly interact with many intracellular proteins and transcription factors,[13,39] and this interaction increases stability[13,40]

or inactivates/interferes with the cellular functions[41] of those target proteins. In our study, the proteomic analysis followed by immunoprecipitation assessment found that ABRO1 binds to METTL3, and this interaction affects the m⁶A methylation function of METTL3 without modulating its expression level. Currently, the underlying mechanism of ABRO1-dependent inhibition of METTL3 activity is unknown. One possibility is that ABRO1 could promote deubiquitylation of METTL3 and blocking of its activity. Most importantly, it is currently unknown how ABRO1 is suppressed in the neonatal heart and which factors are involved in its upregulation in young and adult hearts. Further follow-up studies are warranted to resolve these questions.

M⁶A modification of mRNA, a mechanism regulating post-transcriptional processing and translation of protein, controls the cardiac gene expression program and signaling molecules associated with cardiac physiological functions as well as pathological disorders.[21,22] METTL3-mediated N6-methyladenosine modification is the most abundant epigenetic modification in eukaryotic mRNAs and METTL3 is required for cardiac homeostasis and handling hypertrophic stress response in the mammalian heart.[23] However, its role in heart development, especially in cardiac proliferation, is largely unknown. In our study, the transcriptome-wide m⁶A sequencing analysis in ABRO1 KO hearts showed that METTL3-induced m⁶A hypermethylation of PSPH mRNA is associated with the enhanced translation of PSPH mRNA, which is evident from the remarkable increase of PSPH mRNA and protein levels. METTL3-dependent m⁶A methylation of gene transcripts can either positively or negatively regulate its stability and translation, which depends on the vicinity of METTL3 binding m⁶A peaks in mRNAs.[21,42–44] The enrichment of m⁶A peaks within the proximity of stop codons or the starting of 3′ UTR promotes METTL3-mediated translation of mRNA transcripts.[42,44] Inconsistent with this, we observed the abundance of m⁶A peak in the CDS region in PSPH mRNA from ABRO1 KO hearts, and it correlates with an increased level of PSPH protein. Interestingly, the increased level of PSPH is associated with cardiomyocyte proliferation in the injured postnatal hearts. Recent studies demonstrate that PSPH promotes cell cycle progression and positively regulates cell proliferation,[32,33,35,36] which presumably occurs through upregulation or activation of cell cycle-associated proteins[32]; however, its functional relevance in the cell cycle remains largely unknown. Given that PSPH principally functions as a dephosphorylating enzyme, we performed phosphoproteomic analysis in PSPH-silenced cardiomyocytes and found that CDK2, a kinase protein mainly involved in G2/S transition phase, mitosis, and cell cycle

Figure 5. Transcriptome-wide m⁶A methylome analyses (using m⁶A-Seq) in ABRO1 KO mice heart

(A) LC-MS/MS analysis in FLAG-ABRO1 immunopurified protein complex identified METTL3. (B and C) Immunoprecipitation assessment using anti-METTL3 antibody (B) and anti-ABRO1 antibody (C) showing the interaction of ABRO1 and METTL3. Representative immunoblots from four independent experiments with similar results. (D) Pie chart showing the distribution of m⁶A peaks in different non-overlapping segments (5′ UTR), start codon site (start C), coding sequence (CDS), stop codon site (stop C), and 3′ UTR of mRNA transcripts in WT and ABRO1 KO mouse hearts. (E) Sequence motifs enriched within m⁶A peaks identified by Methylated RNA Immunoprecipitation with Next Generation Sequencing (MeRIP-seq) in ABRO1 KO mouse hearts. (F) Scatterplot showing the m⁶A enrichment in mRNAs of WT and ABRO1 KO mouse hearts. m⁶A-containing mRNAs with significantly increased (up) and decreased peak (down) enrichment are highlighted in red and blue, respectively. (G) Correlation between the level of gene expression and changes in m⁶A level in ABRO1 KO mouse hearts compared with WT hearts. All data are mean ± SD.
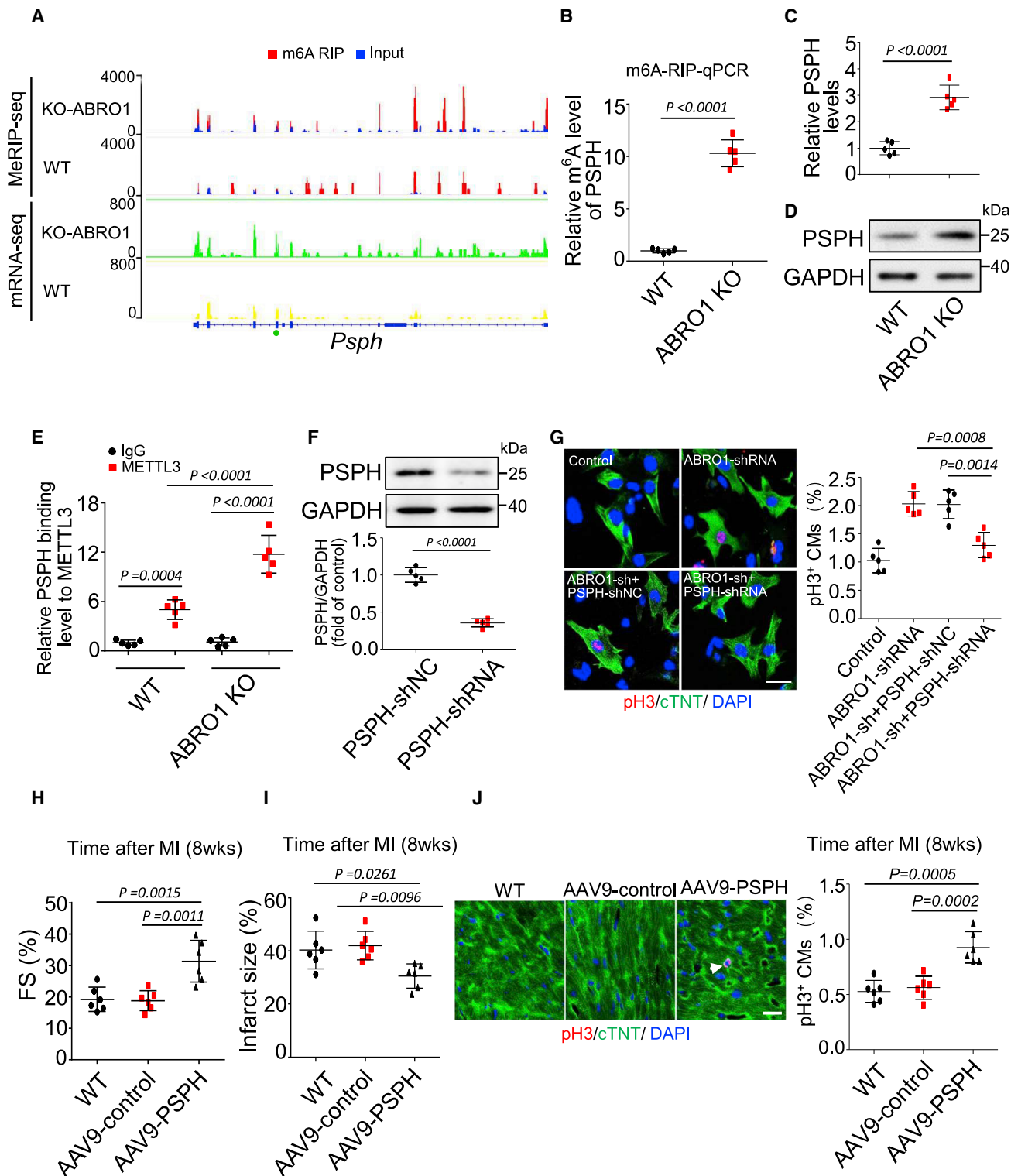
Figure 6. ABRO1 KO promotes METTL3-dependent m⁶A methylation of phosphoserine phosphatase (PSPH) and its expression

(A) Integrative Genomics Viewer (IGV) tracks showing MeRIP-seq (top) and mRNA-seq (bottom) read distribution in *Psph* mRNA from ABRO1 KO and WT mouse hearts. (B) MeRIP-qPCR validation of m⁶A enrichment level in PSPH mRNA in WT and ABRO1 KO hearts (n = 5 mice per group). (C and D) Expression levels of

(legend continued on next page)

progression, is phospho-modified at Thr14 and Tyr15 sites. The phosphorylation level of CDK2 at Thr14 and Tyr15, the two regulatory sites involved in controlling CDK2 catalytic activity and abnormalities of cell cycle,[37,38,45] are remarkably increased upon PSPH silencing or ABRO1 OE and significantly decreased upon PSPH overexpression or ABRO1 silencing in cardiomyocytes and postnatal heart. Further, the reversal of ABRO1-shRNA mediated increase of CDK2 (Thr14/Tyr15) dephosphorylation in the absence of PSPH reveals that ABRO1 functions as a regulator of PSPH in cardiomyocytes. It is well established that the cardiac-specific re-expression of CDK2 in the adult can increase the cardiomyocyte populations' proliferating capability, which is characterized by smaller mononucleated cells along with upregulation of activity of other cell cycle proteins.[8] Consistent with this, the increased activity of CDK2, indicated by reduced Thr14/Tyr15 phosphorylation, in ABRO1 KO heart is accompanied by a reduction of cardiomyocytes size as well as the increase of proliferating cardiomyocytes population in postnatal hearts. Notably, the increase of cardiomyocyte size and significantly reduced cardiomyocyte numbers with proliferative markers is accompanied by the reduction of CDK2 activity in ABRO1 OE neonatal hearts, indicating that ABRO1 promotes cell cycle withdrawal and non-proliferative growth of cardiomyocytes. Further studies are warranted to decipher whether ABRO1 is associated with physiological and/or pathological hypertrophic responses.

Altogether, our findings reveal that ABRO1, the component of the K63-deubiquitinating system, is an important regulator of postnatal cardiomyocyte proliferation and cardiac muscle regeneration in the adult heart. Intriguingly, METTL3-dependent m[6]A hypermethylation of PSPH mRNA, an upregulation of PSPH proteins, and PSPH-mediated activation of CDK2, which is a newly identified mechanism, can promote cell cycle progression, cardiomyocyte proliferation, and cardiac regeneration in postnatal and adult hearts. However, the upregulation of ABRO1, through a currently unknown mechanism, in the myocardial tissue during the postnatal life affects this signaling and results in cardiomyocyte cycle arrest. Thus, our study provides an important clue to understanding why the adult cardiomyocytes lose their proliferative capacity and how the adult cardiac muscle tissue loses its regenerative potential. Given that reinstating the proliferative ability of cardiomyocytes in the adult heart is one of the most effective therapeutic approaches for cardiac regeneration and repair, the efficient cardiac regeneration along with a significant improvement of the heart function upon ABRO1 silencing in the MI-injured hearts suggest that ABRO1, a master regulator of

many signaling pathways, could be a potential target to enforce cardiomyocyte proliferation and cardiac regeneration in diseased adult heart.

MATERIALS AND METHODS

Animals
C57BL/6 mice were used in this study. All the experiments were performed on mice with similar age and body weight, and mice with normal physiological index during surgical procedures were used for analyses.

Generation of ABRO1 KO mice
ABRO1 KO mice were established by using the CRISPR-Cas9 gene-editing system (Cyagen Biosciences, China). The mixture of plasmids carrying sgRNA1 and sgRNA2 was microinjected along with Cas9 mRNA into the fertilized eggs from C57BL/6 mice and the eggs were cultivated overnight. Then, they were transplanted into the oviducts of pseudopregnant recipient females. The founder lines were identified through PCR genotyping of the offspring's tail DNA and further confirmed through direct Sanger sequencing. The following primer sequences were used to amplify the genomic DNA fragments containing the CRISPR-Cas9 target sites and *ABRO1* KO. The forward primer (F1) was 5′-CTCAGTTAAGGTACCGTTTG-3′, the reverse primer (R1) was 5′-TGAGAGTGTGTGTGGGGGTGAG-3′, and the reverse primer (R2) was 5′-GCTGGTGTCATCTATTAATAGG-3′.

MI in heart
MI was induced by ligation of the left anterior descending coronary artery (LAD) as described previously.[46] In brief, the animal is intubated and an animal ventilator (DHX-50, Chengdu Instrument Factory, China) is used to maintain normal breathing. The thoracotomy was performed between the third and fourth ribs, and the chest expander opened the chest cavity to expose the heart. The LAD was ligated with a silk suture 2–3 mm distal from the ascending aorta using nylon suture (6-0) (China Ningbo Medical Suture Needle Co.) and tied for the induction of MI.

MI surgery was carried out in neonatal mouse pups as previously described.[5,31] Briefly, 1-day-old (P1) pups were randomized and anesthetized by placing on an ice bed for 5–6 min (induces hypothermic circulatory arrest) and lateral thoracotomy was performed by blunt dissection of the intercostal muscles. The LAD was ligated using nylon suture (8-0) (China Ningbo Medical Suture Needle Co.) and

---

PSPH mRNA and protein in WT and ABRO1 KO mouse hearts (n = 5 mice per group). (E) RIP-qPCR analysis showing relative binding level of PSPH mRNA to METTL3 in WT or ABRO1 KO hearts (n = 5 mice per group). (F) Representative western blot (top) and statistical data (bottom) showing the expression of PSPH in cardiomyocytes infected with adenovirus harboring PSPH-shNC or PSPH-shRNA (n = 5 independent experiments). (G) Neonatal cardiomyocytes were co-infected with adenovirus harboring ABRO1-shRNA along with PSPH-shNC or PSPH-shRNA for 48 h. Cardiomyocytes co-stained with pH3 (red), cTnT (green) and DAPI (nucleus, blue) (scale bar, 20 μm) and pH3-positive cells were quantified (n = 5 independent experiments). (H–J) Forced expression of PSPH promotes cardiomyocyte proliferation following MI injury. AAV9 loaded with PSPH gene (AAV9-PSPH) or negative control (AAV9-control) was administered to adult WT mice and subjected to MI, and heart samples were collected at 8 weeks post MI. Echocardiography analysis of ventricle function (FS%) (H) and infarct size (I) at 8 weeks post MI (n = 6 mice per group). (J) Representative confocal images and quantification of pH3-positive cardiomyocytes in heart sections at 8 weeks post MI (scale bar, 25 μm) (n = 6 mice per group). All data are mean ± SD.

A

B

C

D

E

F

G
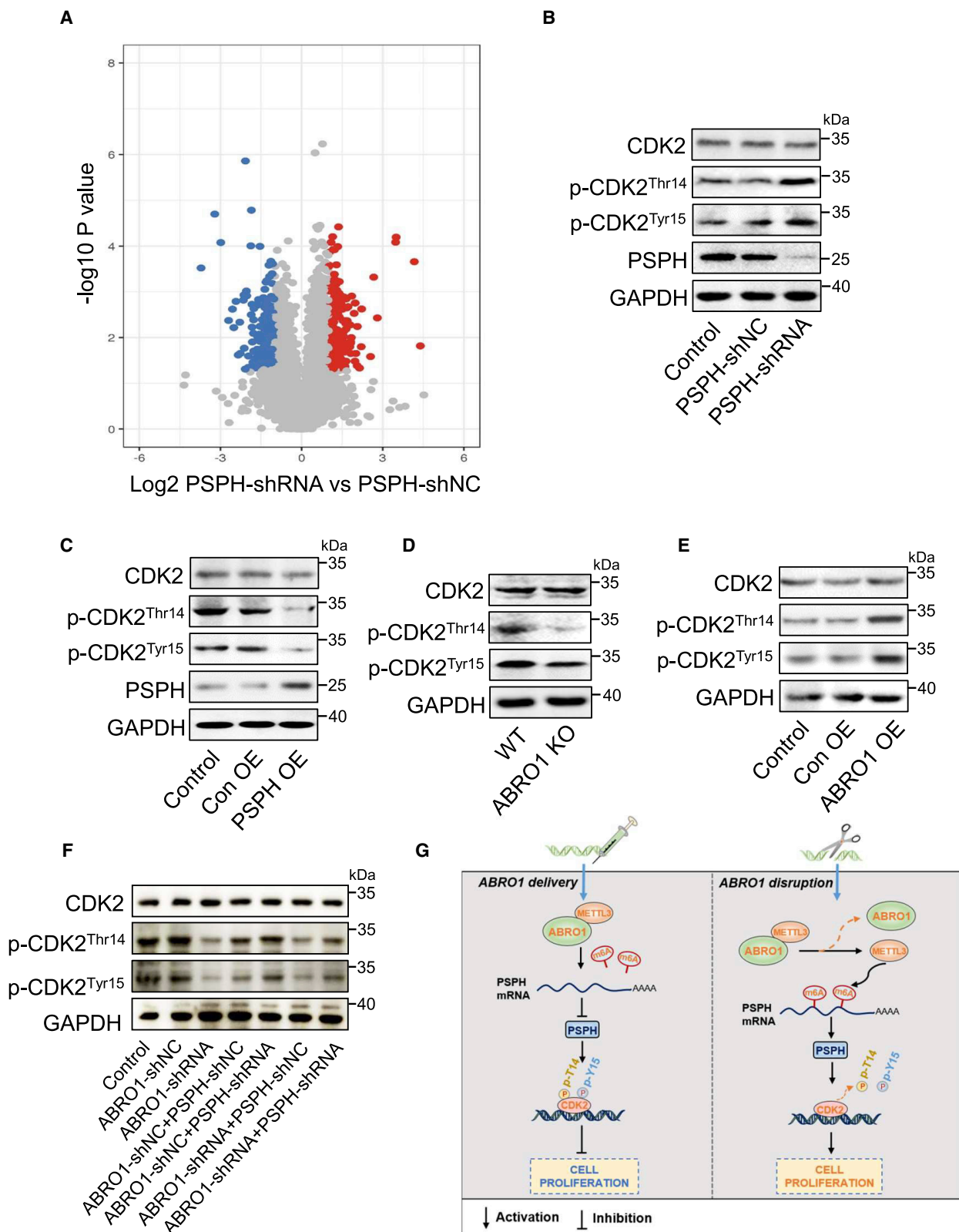
(legend on next page)

tied for the induction of MI. After the LAD, the neonates were transferred from the ice bed, and the thoracic incision and skin wounds were properly closed. Before the skin closure, a small drop of lidocaine (2%) was placed within the incision. After the surgical procedures, the pups were kept under a heat lamp for few minutes for recovery. Then, they were returned to their mothers after waking and becoming active. In the sham group, all the procedures were carried out except the LAD ligation step. The echocardiography measurements and other analyses were carried out at the time points indicated in the figure legends.

For the measurement of infarct size, we calculated MI size by measuring the arc length of the endocardial and epicardial infarcts. Specifically, the NIH ImageJ 1.6 software automatically measures four lengths, including endocardial and epicardium infarct length, and endocardial and epicardium circumference. The endocardial infarct rate was obtained by dividing the endocardial infarct length by the endocardial circumference. The epicardial infarction rate was calculated by the same method. Finally, the MI size was calculated as [(endocardial infarct rate + epicardial infarct rate)/2] × 100.

Echocardiography
Transthoracic echocardiography was performed on lightly anesthetized mice by using a Vevo 2100 Imaging System (VisualSonics, Canada) equipped with a 40-MHz MS-250 scan head. Two-dimensional guided M-mode tracings were recorded in both parasternal long- and short-axis views at the level of the papillary muscles. The fractional shortening (FS) was calculated with the established standard equation. All the measurements were made from more than three beats and averaged.

AAV9 or adenoviral vectors production and administration
Adeno-associated virus serotype 9 (AAV9) was used for ABRO1 OE and PSPH overexpression in the animal model. The AAV9-ABRO1, AAV9-PSPH, and their negative controls were obtained from Hanbio Biotechnology Co. (Shanghai, China). For ABRO1 OE, adult mice were treated with AAV9-PSPH at 2×10^{11} vector genomes (vg)/mouse by tail vein injection. Echocardiography functional analysis was performed at 4 weeks, and the hearts were collected for histological and molecular biological analyses. For PSPH overexpression, adult mice were treated with AAV9-PSPH (2×10^{11} vg/mouse) by tail vein injection before MI. Echocardiography functional analysis was performed at 8 weeks post MI, and the hearts were collected for histological and molecular biological analyses. The adenoviruses harboring ABRO1, ABRO1-shRNA, and their negative controls were obtained from Obio Technology Corp. (Shanghai, China). The adenoviruses harboring PSPH, PSPH-shRNA, and their negative controls were obtained from Hanbio Biotechnology Co. (Shanghai, China). For ABRO1 overexpression, neonatal mice at P1 were treated with adenovirus-ABRO1 (5×10^{10} MOI) by subcutaneous injection, and then the mice were subjected to MI. Echocardiography functional analysis was performed at P7, and the hearts were collected for histological and molecular biological analyses. All experiments were performed according to the protocols approved by the Qingdao University Animal Care Committee.

Neonatal mouse cardiomyocytes isolation and culture
Neonatal cardiomyocytes were isolated from 1- 2-day-old mice according to the previously published protocol.[47] Briefly, carefully take 1- 2-day-old newborn suckling mice into the container and wash 1–2 times with 75% alcohol. The entire process is operated on a clean bench, and the instrument is autoclaved. Open the chest of the suckling mouse with ophthalmological scissors to expose the heart, use small curved forceps to pick and clamp the heart into a plate with 1× PBS buffer, and place it on ice. Then, thoroughly wash 2–3 times, and cut the heart tissue into pieces with surgical scissors. the heart tissue is isolated from the atria, split, and digested with 0.2 mg/mL pancreatin (P-3292, Sigma) and 1.0 mg/mL collagenase type II (LS004176, Worthington) at 42°C. Centrifuge the collected digestion products, 1,000 rpm, 5 min, to collect the myocardial cell pellet. They were cultured in DMEM/F12-Dulbecco's modified Eagle's medium (Gibco, USA) with 5% FBS. For the gene overexpression or silencing, cells were infected with adenoviruses carrying the appropriate gene or shRNA, at a specific MOI.

Isolation of adult mouse cardiomyocytes
Adult cardiac cardiomyocytes were isolated using the Langendorff perfusion system. The hearts of mice were removed by thoracotomy, and the aorta was isolated and connected to the Langendorff perfusion system. Hearts were perfused with trypan buffer (137 mM Nacl, 5.4 mM KCl, 1.2 mM MgCl$_2$, 20 mM NaH$_2$PO$_4$, 20 mM HEPES, 10 mM D-glucose, 10 mM taurine, PH = 7.35) until the

Figure 7. Phosphoproteome profiling in PSPH-silenced cardiomyocytes and identification of the potential target of PSPH
(A) LC-MS/MS-based quantitative phosphoproteomic studies in cardiomyocytes infected with PSPH-shRNA or PSPH-shNC. Volcano plot showing significantly altered proteins (enriched with phosphorylation sites) (fold change >2). Gray dots show phosphoproteins without any differences. Red and blue dots show phosphoproteins significantly increased and decreased, respectively. (B–E) ABRO1 and PSPH regulate CDK2 activity. The immunoblots showing the levels of total CDK2, phospho-CDK2 (Thr14), phospho-CDK2 (Tyr15), and PSPH in cardiomyocytes infected with adenovirus harboring PSPH-shNC or PSPH-shRNA (B), in cardiomyocytes infected with adenovirus harboring PSPH OE or Con OE (C), in WT or ABRO1-deleted (ABRO1 KO) mouse hearts (D) and in cardiomyocytes infected with adenovirus harboring Con OE or ABRO1 OE (E). (F) PSPH silencing reverses the effect of ABRO1-shRNA on CDK2 phosphorylation in cardiomyocytes. Neonatal cardiomyocytes were co-infected with adenovirus harboring ABRO1-shRNA along with PSPH-shNC or PSPH-shRNA for 48 h. Representative immunoblots showing the levels of total CDK2, phospho-CDK2 (Thr14), phospho-CDK2 (Tyr15), and PSPH proteins (n = 5 independent experiments). (G) Schematic diagram showing ABRO1-mediated regulation of METTL3 activity and cardiomyocyte proliferation. In the adult heart, the expression of ABRO1 blocks METTL3-dependent m6A methylation of PSPH mRNA, which results in decreased expression of PSPH proteins and inhibition of CDK2 activity (a cell cycle protein involved in G1/S, S/G2, and G2/M phase) by increased phosphorylation at Thr14 and Tyr15. This leads to cell cycle arrest in cardiomyocytes, while silencing of ABRO1 can accelerate cardiomyocyte proliferation by suppressing PSPH-mediated inhibition of CDK2 activity. All data are mean ± SD.

residual blood was completely pumped. Hearts were digested with collagenase type II (0.1 mg/mL, Worthington) for 16 min at 37°C until they were pale and flaccid. At the end of digestion, the digested hearts were transferred to a 6-cm dish, and the heart tissue was torn with forceps to form 3- to 5-mm tissue blocks. The cells were gently blown to accelerate separation, then filtered through a 100-μm filter. The collected cells were centrifuged at 500 rpm for 1 min to collect cardiomyocytes, and the supernatant was removed. The cells were resuspended using 10 mL of M199 medium and added to laminin-coated culture plates (5 μg/mL) for 2 h at 37°C. Adherent cardiomyocytes were used for immunofluorescence staining experiments.

Analysis of cardiomyocyte nucleation and ploidy

Cardiomyocytes were isolated from WT and ABRO1 KO mice and then fixed with paraformaldehyde, permeabilized, and blocked successively. At the end of blocking, cardiomyocytes were labeled with mouse anti-cardiomyocyte-specific troponin T (anti-cTNT, 1:800, Abcam) and nuclei were labeled with 4',6'-diamidino-phenylindole (DAPI, 1:1,000, Invitrogen). Cardiomyocyte nucleation and ploidy analyses were performed using laser confocal microscopy. In the same section, nuclear ploidy normalization statistics were performed by the difference in DAPI fluorescence intensity between cardiomyocytes and non-cardiomyocytes. ImageJ was used to measure DAPI fluorescence intensity in individual nuclei. The average fluorescence intensity of DAPI in non-myocardial nuclei was used as the diploid nucleus standard. The normalized intensity values of cardiomyocyte nuclei in the range of 0.5–1.5 times the standard were diploid, and the normalized intensity values of cardiomyocyte nuclei in the range of 1.5–2.5 times the standard were tetraploid. Cardiomyocyte nuclei with normalized intensity values greater than 2.5 times this standard range were considered polyploid.

Histological analyses

After the experimental period, the hearts were fixed in 4% paraformaldehyde (prepared in PBS) overnight and they were embedded in paraffin after a series of ethanol dehydration. The tissues sections (7-μm thickness) were stained with hematoxylin and eosin (H&E) (C0105, Beyotime, Shanghai, China) according to the standard protocol. To determine cardiac fibrosis, we stained the heart sections with standard Masson trichrome staining according to manufacturer's instructions (G1340, Solarbio, Beijing, China). For EdU labeling experiments *in vivo*, the adult mice were injected intraperitoneally with EdU (5 mg/kg) every 2 days for 6 days. EdU staining was performed with YF594 Click-iT EdU Imaging Kits (C6017,UE) according to the manufacturer's instructions.

Apoptosis assays

Cardiomyocyte apoptosis was determined by TUNEL using a kit (40307ES20, Yeasen). Cultured cells and tissue sections were performed for TUNEL staining assays according to the kit instructions.

Immunofluorescence staining and analyses

The heart tissue was embedded in optimal cutting temperature compound (OCT) and placed at −20°C. The frozen sectioned tissue was taken out to dry at room temperature for 15 min, then washed with 1× PBS buffer to remove OCT for 3 min each time. The treated cells and heart tissue were fixed in 4% paraformaldehyde for 15 min and washed three times with 1× PBS buffer. The sample was permeated by 0.5% Triton X-100 (prepared in 1× PBS buffer) for 15 min at room temperature. After washing with PBS, the sample was blocked with 2% BSA for 30 min. The blocking solution was discarded and the primary antibody added at room temperature for 2 h or 4°C overnight. For the detection of mitosis and cytokinesis, rabbit anti-phospho-histone H3 (pH3, 1:200, Abcam) and anti-Aurora B (1:200, Abcam) antibodies were used. The cardiomyocytes were labeled with mouse anti-cTNT (1:800, Abcam) and DAPI (1:1,000, Invitrogen) was used to label nuclei. The tetraethyl rhodamine isothiocyanate (TRITC)-conjugated anti-rabbit immunoglobulin G (IgG) (111-025-003, 1:200, Jackson) and the FITC-conjugated anti-mouse IgG (115-095-003, 1:200, Jackson) were used for fluorescence secondary antibody staining. After washing with PBS, DAPI was stained for 5 min and anti-fluorescence quencher added dropwise, observed, and pictures taken under a laser confocal microscope. For the calculation of cell cross-sectional area, the heart sections were stained with FITC-conjugated wheat germ agglutinin (Sigma, St. Louis, MO) as previously described.[48] The length of cardiomyocytes was measured along their long axis, and cell width was measured along the cross section at their midpoint from images captured using confocal microscope (LSCM, Leica, Germany).

Immunoblot and immunoprecipitation

Immunoblot was performed as previously described.[49] In short, treated cardiomyocytes and heart tissue were lysed for 30 min by using Radio-Immunoprecipitation Assay (RIPA) buffer (R0020, Solarbio) containing protease inhibitor PMSF. All protein lysis samples were fractionated in 10%–12% SDS-PAGE gels and transferred to nitrocellulose membranes. The membranes were incubated with 5% skimmed milk at room temperature for 1 h, and western blots were probed overnight at 4°C using the primary antibodies. The following antibodies were used: ABRO1(NBP1-90282, Novusbio), METTL3 (15073-1-AP, ProteinTech), PSPH (A7924, ABclonal), CDK1 (31007, ZENBIO), CDK2 (380676, ZENBIO), phospho-CDK2 (Thr14) (bs-5277R, Bioss), phospho-CDK2 (Tyr15) (382901, ZENBIO), CDK4 (R23886, ZENBIO), Cyclin B1 (A19037, ABclonal), Cyclin D1 (A19038, ABclonal), P53 (2524S, CST), P27 (ab193379, Abcam), P21 (ab109199, Abcam) and YAP1 (NB110-58358, Novusbio). Anti-glyceraldehyde-3-phosphate dehydrogenase (GAPDH) was obtained from Absin (abs132004). The horseradish peroxidase-conjugated secondary antibodies (anti-mouse, anti-rabbit, or anti-goat) were obtained from Absin. The membranes were incubated with enhanced chemiluminescence detection kit (ECL, E411-04, Vazyme) and developed with a scanning imager (Fusion solo 4s.wl, Vilber lourmat).

The cultured primary cardiomyocytes were collected and lysed using immunoprecipitation (IP) buffer (270 mM NaCl, 40 mM Tris-HCl, 1 mM EDTA, 2% NP40, 20% glycerol, protease inhibitor, and phosphatase inhibitor). The equal concentration of samples was incubated with antibodies (ABRO1 and METTL3) or IgG overnight at 4°C. The

protein A/G agarose (sc-2003, Santa Cruz) was added and kept at 4°C for 4 h with gentle agitation, coupling antibody to sepharose beads. After the immunoprecipitation reaction, the co-precipitated complex was centrifuged at 3,000 rpm for 3 min at 4°C, and the agarose beads were centrifuged to the bottom of the tube. Then, the collected samples were washed three times with lysis buffer, adding 25 μL of 2× SDS loading buffer, and boiled for 5 min. Finally, the samples were analyzed by SDS-PAGE, western blotting, and mass spectrometry.

qRT-PCR

The total RNA was extracted (Trizol reagent 15596-026, Invitrogen, USA) and treated with DNAse I (Takara, Japan). They were subjected to reverse transcription using reverse transcriptase (ReverTra Ace, Toyobo, Japan), and amplified using the SYBR Premix Ex Taq II kit (Takara, Japan). qPCR was performed on a CFX96 Real-Time PCR Detection System (Bio-Rad). After the PCR reaction, the amplification curve and melting curve were immediately analyzed. The following sequences of primers were used for qRT-PCR analysis: ABRO1 forward primer was 5′-CAGCTTCATCTCTACCGCCA-3′; the reverse primer was 5′-TGAGACGTGTTTGGCACTGA-3′. PSPH forward was 5′-GCAGTGTGCTTTGATGTTGA-3′; PSPH reverse, 5′-ATGGCTCTCCGTGTCATTT-3′. KIM-1 forward was 5′-ACATATCGTGGAATCACAACGAC-3′; KIM-1 reverse, 5′-ACTGCTCTTCTGATAGGTGACA-3′. Nppa forward, 5′-GCTTCCAGGCCATATTGGAG-3′; Nppa reverse, 5′-GGGGGCATGACCTCATCTT-3′. Myh7 forward, 5′-ACTGTCAACACTAAGAGGGTCA-3′; Myh7 reverse, 5′-TTGGATGATTTGATCTTCCAGGG-3′. GAPDH was used as an internal control and all the results were normalized to GAPDH. GAPDH forward primer was 5′-CAGTGGCAAAGTGGAGATTGTTG-3′; the reverse primer was 5′-TCGCTCCTGGAAGATGGTGAT-3′.

Mass spectrometry analysis

The FLAG-tagged ABRO1 adenovirus was infected into cardiomyocytes and immunoprecipitation was performed to pull down the ABRO1 binding proteins with Anti-FLAG M2 Magnetic Beads (Sigma-Aldrich). FLAG-ABRO1-bound products were resolved using SDS-PAGE gel and stained with Coomassie blue. The extracted band was sent to a commercial facility for the LC-MS/MS analysis (Shanghai Applied Protein Technology Company, Shanghai, China).

RIP assay

RIP was performed as previously described.[50] The ventricle sections of WT and ABRO1 KO were treated with 1% formaldehyde (for crosslinking) and tissue lysate was prepared using RIPA buffer (Cell Signaling Technology, USA) mixed with 1 mM PMSF, 1× proteinase inhibitor cocktail (Roche), and 1% RNaseOUT (Invitrogen). The whole tissue lysate was incubated with anti-METTL3 and IgG at 4°C overnight. The RNA/protein complex was recovered using protein G Dynabeads and washed gently with RIPA buffer several times. Then, they were reverse crosslinked with proteinase K at 50°C for 60 min, and the protein-bound RNA was analyzed by RT-PCR after extraction using Trizol reagent.

MeRIP-seq

RNA was extracted from WT and ABRO1 KO mouse hearts and quantified (using NanoDrop ND-1000). m^6A RNA-seq service was provided by Cloudseq Biotech (Shanghai, China). Briefly, m^6A RNA immunoprecipitation was performed with the GenSeq m^6A RNA immunoprecipitation kit (GenSeq, China) by following the manufacturer's instructions. Both the input sample without immunoprecipitation and the m^6A immunoprecipitation samples were used for RNA-seq library generation with NEBNext Ultra II Directional RNA Library Prep Kit (New England Biolabs, USA). The library quality was evaluated with BioAnalyzer 2100 system (Agilent Technologies, USA). Library sequencing was performed on an Illumina HiSeq instrument with 150-bp paired-end reads. Paired-end reads were harvested from the Illumina HiSeq 4000 sequencer, and were quality controlled by Q30, followed by 3′ adaptor trimming and low-quality read removal by cutadapt software (v1.9.3). First, clean reads of all libraries were aligned to the reference genome (UCSC MM10) by Hisat2 software (v2.0.4). Methylated sites on RNAs (peaks) were identified by MACS software. Differentially methylated sites were identified by diffReps. These peaks identified by both softwares overlapping with exons of mRNA were figured out and chosen by homemade scripts. GO and pathway enrichment analysis were performed by the differentially methylated protein coding genes.

m^6A-RIP-qPCR

The DNAase-treated RNA samples (100 μg) were incubated with m6A-antibody-bound protein G beads (pre-blocked with 1% BSA) in immunoprecipitation buffer (150 mM NaCl, 10 mM Tris-HCl, and 0.1% NP-40 containing protease and RNAse inhibitor) overnight at 4°C with gentle rotation. The beads were washed with immunoprecipitation buffer the next day and RNA was eluted (two times) using m6A-free nucleotide solution. Then, elute (rich in m6A-enriched transcripts) was subjected to phenol-chloroform extraction for RNA purification, and qRT-PCR analysis was carried out.

Global proteomic and phosphoproteomic analysis

For the quantitative analysis of proteomics and phosphoproteomics, the samples were prepared and treated as previously described.[51,52] In brief, the lysate of cardiomyocytes infected with adenovirus PSPH-shRNA and its control were sonicated three times on ice using a high-intensity ultrasonic processor (Scientz) in lysis buffer (8 M urea, 1% protease inhibitor cocktail). For digestion, the protein solution was reduced with 5 mM dithiothreitol for 30 min at 56°C and alkylated with 11 mM iodoacetamide for 15 min at room temperature in darkness. The protein sample was then diluted by adding 100 mM Triethanolamine Buffer (TEAB) to urea concentration less than 2 M. Finally, trypsin was added at 1:50 trypsin-to-protein mass ratio for the first digestion overnight and 1:100 trypsin-to-protein mass ratio for a second 4-h digestion. Peptide mixtures were first incubated with IMAC microsphere suspension with vibration in loading buffer (50% acetonitrile/6% trifluoroacetic acid). The IMAC microspheres with enriched phosphopeptides were collected by centrifugation, and the supernatant was removed. To remove nonspecifically adsorbed peptides, the IMAC microspheres were washed with 50%

acetonitrile/6% trifluoroacetic acid and 30% acetonitrile/0.1% trifluoroacetic acid, sequentially. To elute the enriched phosphopeptides from the IMAC microspheres, elution buffer containing 10% NH4OH was added and the enriched phosphopeptides were eluted with vibration. The supernatant containing phosphopeptides was collected and lyophilized for LC-MS/MS analysis.

The enriched phosphopeptides were subjected to tandem mass spectrometry (MS/MS) in a Q Exactive Plus mass spectrometer (Thermo Scientific). The resulting MS/MS data were processed using Maxquant search engine (v.1.5.2.8). Tandem mass spectra were searched against mouse UniProt database concatenated with reverse decoy database. Trypsin/P was specified as the cleavage enzyme, allowing up to four missing cleavages. The mass tolerance for precursor ions was set as 20 ppm in the first search and 5 ppm in the main search, and the mass tolerance for fragment ions was set as 0.02 Da. Carbamidomethylation of Cys was specified as a fixed modification, and oxidation of Met; phosphorylation of Ser, Thr, and Tyr; and acetylation modification were specified as variable modifications. False discovery rate (FDR) was adjusted to <1% and minimum score for modified peptides was set >40.

Statistical analysis

All data are presented as mean ± SD. GraphPad Prism software package (GraphPad) was used for statistical analyses. Student's t test was used for the comparison of statistical significance between two groups, and all tests were determined by unpaired two-sided tests. Comparisons between multiple groups were assessed by one-way ANOVA with Tukey's multiple comparisons test or two-way ANOVA with Bonferroni's multiple comparisons test. $p < 0.05$ was considered statistically significant.

DATA AVAILABILITY

The data that support the findings of this study are available from the corresponding author upon reasonable request.

SUPPLEMENTAL INFORMATION

Supplemental information can be found online at https://doi.org/10.1016/j.ymthe.2023.01.011.

AUTHOR CONTRIBUTIONS

K.W., K.Y., and C.L. designed and supervised the experiments. T.W., L.Z., X.L., F.L., L.L., X.C., J.J., M.P., and K.W. performed experiments. T.W., L.Z., X.L., F.L., L.L., and X.C. analyzed the data. K.W., K.Y., C.L., T.W., and M.P. wrote the manuscript.

REFERENCES

1. Kang, M.J., and Koh, G.Y. (1997). Differential and dramatic changes of cyclin-dependent kinase activities in cardiomyocytes during the neonatal period. J. Mol. Cell. Cardiol. 29, 1767–1777.

2. Ponnusamy, M., Li, P.F., and Wang, K. (2017). Understanding cardiomyocyte proliferation: an insight into cell cycle activity. Cell. Mol. Life Sci. 74, 1019–1034.

3. Mollova, M., Kühn, B., Bersell, K., Walsh, S., Savla, J., Das, L.T., Park, S.Y., Silberstein, L.E., Dos Remedios, C.G., Graham, D., et al. (2013). Cardiomyocyte proliferation contributes to heart growth in young humans. Proc. Natl. Acad. Sci. USA 110, 1446–1451.

4. Naqvi, N., Li, M., Calvert, J.W., Tejada, T., Lambert, J.P., Wu, J., Kesteven, S.H., Holman, S.R., Matsuda, T., Lovelock, J.D., et al. (2014). A proliferative burst during preadolescence establishes the final cardiomyocyte number. Cell 157, 795–807.

5. Porrello, E.R., Mahmoud, A.I., Simpson, E., Hill, J.A., Richardson, J.A., Olson, E.N., and Sadek, H.A. (2011). Transient regenerative potential of the neonatal mouse heart. Science 331, 1078–1080.

6. Bergmann, O., Bhardwaj, R.D., Bernard, S., Zdunek, S., Barnabé-Heider, F., Walsh, S., Zupicich, J., Alkass, K., Buchholz, B.A., Druid, H., et al. (2009). Evidence for cardiomyocyte renewal in humans. Science 324, 98–102.

7. Mohamed, T.M.A., Ang, Y.S., Radzinsky, E., Zhou, P., Huang, Y., Elfenbein, A., Foley, A., Magnitsky, S., and Srivastava, D. (2018). Regulation of cell cycle to stimulate adult cardiomyocyte proliferation and cardiac regeneration. Cell 173, 104–116.e12.

8. Liao, H.S., Kang, P.M., Nagashima, H., Yamasaki, N., Usheva, A., Ding, B., Lorell, B.H., and Izumo, S. (2001). Cardiac-specific overexpression of cyclin-dependent kinase 2 increases smaller mononuclear cardiomyocytes. Circ. Res. 88, 443–450.

9. Tamamori-Adachi, M., Takagi, H., Hashimoto, K., Goto, K., Hidaka, T., Koshimizu, U., Yamada, K., Goto, I., Maejima, Y., Isobe, M., et al. (2008). Cardiomyocyte proliferation and protection against post-myocardial infarction heart failure by cyclin D1 and Skp2 ubiquitin ligase. Cardiovasc. Res. 80, 181–190.

10. Di Stefano, V., Giacca, M., Capogrossi, M.C., Crescenzi, M., and Martelli, F. (2011). Knockdown of cyclin-dependent kinase inhibitors induces cardiomyocyte re-entry in the cell cycle. J. Biol. Chem. 286, 8644–8654.

11. Cooper, E.M., Cutcliffe, C., Kristiansen, T.Z., Pandey, A., Pickart, C.M., and Cohen, R.E. (2009). K63-specific deubiquitination by two JAMM/MPN+ complexes: BRISC-associated Brcc36 and proteasomal Poh1. EMBO J. 28, 621–631.

12. Cooper, E.M., Boeke, J.D., and Cohen, R.E. (2010). Specificity of the BRISC deubiquitinating enzyme is not due to selective binding to Lys63-linked polyubiquitin. J. Biol. Chem. 285, 10344–10352.

13. Zhang, J., Yang, X., Cao, M., Dong, J., Li, C., Xu, W., Zhan, Y., Wang, X., Yu, M., Ge, C., et al. (2014). ABRO1 suppresses tumourigenesis and regulates the DNA damage response by stabilizing p53. Nat. Commun. 5, 5059.

14. Ren, G., and Zhang, X. (2019). ABRO1 promotes NLRP3 inflammasome activation through regulation of NLRP3 deubiquitination. EMBO J. 38, e100376.

15. Xu, S., Wu, X., Wu, L., Castillo, A., Liu, J., Atkinson, E., Paul, A., Su, D., Schlacher, K., Komatsu, Y., et al. (2017). Abro1 maintains genome stability and limits replication stress by protecting replication fork stability. Genes Dev. 31, 1469–1482.

16. Yan, K., Li, L., Wang, X., Hong, R., Zhang, Y., Yang, H., Lin, M., Zhang, S., He, Q., Zheng, D., et al. (2015). The deubiquitinating enzyme complex BRISC is required for proper mitotic spindle assembly in mammalian cells. J. Cell Biol. 210, 209–224.

17. Cilenti, L., Balakrishnan, M.P., Wang, X.L., Ambivero, C., Sterlicchi, M., del Monte, F., Ma, X.L., and Zervos, A.S. (2011). Regulation of Abro1/KIAA0157 during myocardial infarction and cell death reveals a novel cardioprotective mechanism for Lys63-specific deubiquitination. J. Mol. Cell. Cardiol. 50, 652–661.

18. Quaife-Ryan, G.A., Sim, C.B., Ziemann, M., Kaspi, A., Rafehi, H., Ramialison, M., El-Osta, A., Hudson, J.E., and Porrello, E.R. (2017). Multicellular transcriptional analysis of mammalian heart regeneration. Circulation 136, 1123–1139.

19. Hu, P., Liu, J., Zhao, J., Wilkins, B.J., Lupino, K., Wu, H., and Pei, L. (2018). Single-nucleus transcriptomic survey of cell diversity and functional maturation in postnatal mammalian hearts. Genes Dev. 32, 1344–1357.

20. Wang, Z., Olson, E.N., Cui, M., Shah, A.M., Ye, W., Tan, W., Min, Y.L., Botten, G.A., Shelton, J.M., Liu, N., et al. (2019). Mechanistic basis of neonatal heart regeneration revealed by transcriptome and histone modification profiling. Proc. Natl. Acad. Sci. USA 116, 18455–18465.

21. Kmietczyk, V., Riechert, E., Kalinski, L., Boileau, E., Malovrh, E., Malone, B., Gorska, A., Hofmann, C., Varma, E., Jurgensen, L., et al. (2019). m(6)A-mRNA methylation regulates cardiac gene expression and cellular growth. Life Sci. Alliance 2, e201800233.

22. Berulava, T., Buchholz, E., Elerdashvili, V., Pena, T., Islam, M.R., Lbik, D., Mohamed, B.A., Renner, A., von Lewinski, D., Sacherer, M., et al. (2020). Changes in m6A RNA methylation contribute to heart failure progression by modulating translation. Eur. J. Heart Fail. 22, 54–66.

23. Dorn, L.E., Lasman, L., Chen, J., Xu, X., Hund, T.J., Medvedovic, M., Hanna, J.H., van Berlo, J.H., and Accornero, F. (2019). The N(6)-methyladenosine mRNA methylase METTL3 controls cardiac homeostasis and hypertrophy. Circulation 139, 533–545.

24. Mathiyalagan, P., Adamiak, M., Mayourian, J., Sassi, Y., Liang, Y., Agarwal, N., Jha, D., Zhang, S., Kohlbrenner, E., Chepurko, E., et al. (2019). FTO-dependent N(6)-methyladenosine regulates cardiac function during remodeling and repair. Circulation 139, 518–532.

25. Liddy, K.A., White, M.Y., and Cordwell, S.J. (2013). Functional decorations: post-translational modifications and heart disease delineated by targeted proteomics. Genome Med. 5, 20.

26. Yan, K., Wang, K., and Li, P. (2019). The role of post-translational modifications in cardiac hypertrophy. J. Cell. Mol. Med. 23, 3795–3807.

27. Wang, J., and Schwartz, R.J. (2010). Sumoylation and regulation of cardiac gene expression. Circ. Res. 107, 19–29.

28. Fan, Y., Zhang, Q., Li, H., Cheng, Z., Li, X., Chen, Y., Shen, Y., Wang, L., Song, G., and Qian, L. (2017). Peptidomics analysis of transient regeneration in the neonatal mouse heart. J. Cell. Biochem. 118, 2828–2840.

29. Chakraborty, S., Sengupta, A., and Yutzey, K.E. (2013). Tbx20 promotes cardiomyocyte proliferation and persistence of fetal characteristics in adult mouse hearts. J. Mol. Cell. Cardiol. 62, 203–213.

30. Mahmoud, A.I., Kocabas, F., Muralidhar, S.A., Kimura, W., Koura, A.S., Thet, S., Porrello, E.R., and Sadek, H.A. (2013). Meis1 regulates postnatal cardiomyocyte cell cycle arrest. Nature 497, 249–253.

31. Porrello, E.R., Mahmoud, A.I., Simpson, E., Johnson, B.A., Grinsfelder, D., Canseco, D., Mammen, P.P., Rothermel, B.A., Olson, E.N., and Sadek, H.A. (2013). Regulation of neonatal and adult mammalian heart regeneration by the miR-15 family. Proc. Natl. Acad. Sci. USA 110, 187–192.

32. Bachelor, M.A., Lu, Y., and Owens, D.M. (2011). L-3-Phosphoserine phosphatase (PSPH) regulates cutaneous squamous cell carcinoma proliferation independent of L-serine biosynthesis. J. Dermatol. Sci. 63, 164–172.

33. Nakano, I., Dougherty, J.D., Kim, K., Klement, I., Geschwind, D.H., and Kornblum, H.I. (2007). Phosphoserine phosphatase is expressed in the neural stem cell niche and regulates neural stem and progenitor cell proliferation. Stem Cells 25, 1975–1984.

34. Sun, H.L., Zhu, A.C., Gao, Y., Terajima, H., Fei, Q., Liu, S., Zhang, L., Zhang, Z., Harada, B.T., He, Y.Y., et al. (2020). Stabilization of ERK-phosphorylated METTL3 by USP5 increases m(6)A methylation. Mol. Cell 80, 633–647.e7.

35. Park, S.M., Kim, S.Y., Seo, E.H., Bae, D.H., Kim, S.S., Kim, J., Lin, W., Kim, K.H., Park, J.B., Kim, Y.S., et al. (2019). Phosphoserine phosphatase promotes lung cancer progression through the dephosphorylation of IRS-1 and a noncanonical L-serine-independent pathway. Mol. Cells 42, 604–616.

36. Liao, L., Ge, M., Zhan, Q., Huang, R., Ji, X., Liang, X., and Zhou, X. (2019). PSPH mediates the metastasis and proliferation of non-small cell lung cancer through MAPK signaling pathways. Int. J. Biol. Sci. 15, 183–194.

37. Sebastian, B., Kakizuka, A., and Hunter, T. (1993). Cdc25M2 activation of cyclin-dependent kinases by dephosphorylation of threonine-14 and tyrosine-15. Proc. Natl. Acad. Sci. USA 90, 3521–3524.

38. Hughes, B.T., Sidorova, J., Swanger, J., Monnat, R.J., Jr., and Clurman, B.E. (2013). Essential role for Cdk2 inhibitory phosphorylation during replication stress revealed by a human Cdk2 knockin mutation. Proc. Natl. Acad. Sci. USA 110, 8954–8959.

39. Ambivero, C.T., Cilenti, L., and Zervos, A.S. (2012). ATF4 interacts with Abro1/KIAA0157 scaffold protein and participates in a cytoprotective pathway. Biochim. Biophys. Acta 1823, 2149–2156.

40. Zhao, Y., Yu, Y., Li, H., Zhang, Z., Guo, S., Zhu, S., Guo, Q., Li, P., Min, L., and Zhang, S. (2019). FAM175B promotes apoptosis by inhibiting ATF4 ubiquitination in esophageal squamous cell carcinoma. Mol. Oncol. 13, 1150–1165.

41. An, S., Zhao, L.P., Shen, L.J., Wang, S., Zhang, K., Qi, Y., Zheng, J., Zhang, X.J., Zhu, X.Y., Bao, R., et al. (2017). USP18 protects against hepatic steatosis and insulin resistance through its deubiquitinating activity. Hepatology 66, 1866–1884.

42. Lin, S., Choe, J., Du, P., Triboulet, R., and Gregory, R.I. (2016). The m(6)A methyltransferase METTL3 promotes translation in human cancer cells. Mol. Cell 62, 335–345.

43. Wang, X., Lu, Z., Gomez, A., Hon, G.C., Yue, Y., Han, D., Fu, Y., Parisien, M., Dai, Q., Jia, G., et al. (2014). N6-methyladenosine-dependent regulation of messenger RNA stability. Nature 505, 117–120.

44. Jin, D., Guo, J., Wu, Y., Du, J., Yang, L., Wang, X., Di, W., Hu, B., An, J., Kong, L., et al. (2019). m(6)A mRNA methylation initiated by METTL3 directly promotes YAP translation and increases YAP activity by regulating the MALAT1-miR-1914-3p-YAP axis to induce NSCLC drug resistance and metastasis. J. Hematol. Oncol. 12, 135.

45. D'Angiolella, V., Costanzo, V., Gottesman, M.E., Avvedimento, E.V., Gautier, J., and Grieco, D. (2001). Role for cyclin-dependent kinase 2 in mitosis exit. Curr. Biol. 11, 1221–1226.

46. Ponnusamy, M., Liu, F., Zhang, Y.H., Li, R.B., Zhai, M., Liu, F., Zhou, L.Y., Liu, C.Y., Yan, K.W., Dong, Y.H., et al. (2019). Long noncoding RNA CPR (cardiomyocyte proliferation regulator) regulates cardiomyocyte proliferation and cardiac repair. Circulation 139, 2668–2684.

47. Lin, Z., Murtaza, I., Wang, K., Jiao, J., Gao, J., and Li, P.F. (2009). miR-23a functions downstream of NFATc3 to regulate cardiac hypertrophy. Proc. Natl. Acad. Sci. USA 106, 12103–12108.

48. Dolber, P.C., Bauman, R.P., Rembert, J.C., and Greenfield, J.C., Jr. (1994). Regional changes in myocyte structure in model of canine right atrial hypertrophy. Am. J. Physiol. 267, H1279–H1287.

49. Li, Y.Z., Lu, D.Y., Tan, W.Q., Wang, J.X., and Li, P.F. (2008). p53 initiates apoptosis by transcriptionally targeting the anti-apoptotic protein ARC. Mol. Cell. Biol. 28, 564–574.

50. Tsai, M.C., Manor, O., Wan, Y., Mosammaparast, N., Wang, J.K., Lan, F., Shi, Y., Segal, E., and Chang, H.Y. (2010). Long noncoding RNA as modular scaffold of histone modification complexes. Science 329, 689–693.

51. Wang, J., Qi, L., Huang, S., Zhou, T., Guo, Y., Wang, G., Guo, X., Zhou, Z., and Sha, J. (2015). Quantitative phosphoproteomics analysis reveals a key role of insulin growth factor 1 receptor (IGF1R) tyrosine kinase in human sperm capacitation. Mol. Cell. Proteomics 14, 1104–1112.

52. Wang, M., Guo, Y., Wang, M., Zhou, T., Xue, Y., Du, G., Wei, X., Wang, J., Qi, L., Zhang, H., et al. (2017). The glial cell-derived neurotrophic factor (GDNF)-responsive phosphoprotein landscape identifies raptor phosphorylation required for spermatogonial progenitor cell proliferation. Mol. Cell. Proteomics 16, 982–997.